haematologica
Journal of the Ferrata Storti Foundation

SLC25A1 reprograms mitochondrial and fatty acid metabolism to promote the progression of acute myeloid leukemia

by Miao Chen, Wenze Li, Yuan Tao, Chenglong Hu, Rui Ge, Sijing Kang, Pengjie Yue, Cheuk Him Man, Lan Wang and Xiaojing Yan

Received: January 6, 2025.
Accepted: August 7, 2025.

Citation: Miao Chen, Wenze Li, Yuan Tao, Chenglong Hu, Rui Ge, Sijing Kang, Pengjie Yue, Cheuk Him Man, Lan Wang and Xiaojing Yan. SLC25A1 reprograms mitochondrial and fatty acid metabolism to promote the progression of acute myeloid leukemia.
Haematologica. 2025 Sept 4. doi: 10.3324/haematol.2024.287269 [Epub ahead of print]

Publisher's Disclaimer.
E-publishing ahead of print is increasingly important for the rapid dissemination of science.
Haematologica is, therefore, E-publishing PDF files of an early version of manuscripts that have completed a regular peer review and have been accepted for publication.
E-publishing of this PDF file has been approved by the authors.
After having E-published Ahead of Print, manuscripts will then undergo technical and English editing, typesetting, proof correction and be presented for the authors' final approval; the final version of the manuscript will then appear in a regular issue of the journal.
All legal disclaimers that apply to the journal also pertain to this production process.

SLC25A1 reprograms mitochondrial and fatty acid metabolism to promote the progression of acute myeloid leukemia

Miao Chen[1, *], Wenze Li[1, *], Yuan Tao[1, *], Chenglong Hu[2], Rui Ge[1], Sijing Kang[1], Pengjie Yue[1], Cheuk Him Man[3], Lan Wang[2, #], Xiaojing Yan[1, #]

* MC, WL and YT contributed equally as co-first authors.

# LW and XY contributed equally as senior authors.

[1]Department of Hematology, The First Affiliated Hospital of China Medical University, Shenyang, China.

[2]CAS Key Laboratory of Tissue Microenvironment and Tumor, Shanghai Institute of Nutrition and Health, Shanghai Institutes for Biological Sciences, University of Chinese Academy of Sciences, Chinese Academy of Sciences, Shanghai, China

[3]Department of Medicine, Li Ka Shing Faculty of Medicine, The University of Hong Kong, Hong Kong SAR, China;

Running head: SLC25A1 is essential in AML

[#] **Corresponding authors:**
Xiaojing Yan, yanxiaojing_pp@hotmail.com;
Lan Wang, lwang@sinh.ac.cn

Data-sharing statement: For original data, please contact yanxiaojing_pp@hotmail.com.

Availability of data and materials

All data supporting the findings of this study are available within the article, its supplementary information or from the corresponding author upon reasonable request.

Competing interests

The authors declare that they have no competing interests.

Authorship Contributions

Miao Chen designed the research, performed most of experiments and wrote the paper; Wenze Li performed part of experiments and analyzed part of results; Yuan Tao analyzed part of results; Chenglong Hu performed part of animal experiments; Rui Ge performed part of drug experiments; Sijing Kang participated in part of paper writing; Pengjie Yue participated in part of data analysis; Cheuk Him Man directed cell experiments; Lan Wang directed parts of experiments and revised the article; Xiaojing Yan directed the research design, experiment performance and article revision.

Acknowledgments

The authors would like to acknowledge the contributions of all colleagues in Yan's lab and Wang's lab. Thanks to Prof. Chao Ma for designing and producing CTPI3. Thanks to Prof. Xiaojian Sun for supplying the AE9a cell line. Thanks to Prof. Yiping Wang for providing suggestion to article revision.

Funding

This work was supported by grants from Grant of the National Clinical Priority Specialized Department, Young Talent of Liao Ning Revitalization Talents Program (xlyc1807265), Liaoning central guiding local science and technology development

special project (2023JH6/100200006), the National Youth Top-notch Talent of Ten

Thousand Talent Program (2014-253), Translational Research Grant of NCRCH (2020ZKMB06).

Consent for publication

All authors declare to approve the publication.

Abstract

Abnormal metabolic reprogramming is a hallmark of acute myeloid leukemia (AML), contributing to leukemia initiation, progression and drug resistance. The key mitochondrial citrate transporter SLC25A1 plays an essential role in regulating cellular energy metabolism and shows to play an important role in lipid metabolism regulation. However, the role of SLC25A1 in the pathogenesis and aberrant lipid metabolism in AML remain unexplored. In this study, our analysis of public datasets and patient samples revealed that SLC25A1 expression was markedly elevated in AML and was associated with poor prognosis. Knockdown or pharmacological inhibition of SLC25A1 significantly suppressed AML cell proliferation by inducing apoptosis, without affecting cell cycle progression or differentiation. Moreover, SLC25A1 proved vital for AML tumorigenesis *in vivo*. Mechanistically, we demonstrated that SLC25A1 inhibition disrupted citrate homeostasis, leading to mitochondrial dysfunction and reduced fatty acid metabolism. Notably, we developed a novel SLC25A1 inhibitor, CTPI3, which effectively inhibits the progression of AML *in vivo*, and synergizes with venetoclax to kill AML cells by mitochondrial and fatty acid metabolism regulation. In summary, our findings highlight that SLC25A1 plays a vital role of in maintaining AML cell survival and regulating its drug sensitivity, and further developed a more effective novel drug targeting SLC25A1, providing additional therapeutic options for venetoclax-resistant patients and highlighting SLC25A1 as a promising biomarker and therapeutic target for AML.

Introduction

Acute myeloid leukemia (AML) is a group of hematopoietic malignancies, with characteristics of clonal proliferation and apoptosis or differentiation blockade [1, 2]. Unfortunately, patients with AML generally have poor clinical outcomes and high mortality rates, as a result of frequent drug resistance and relapse [3]. Recent studies found that shift in metabolic pathway is driven by oncogene activation or loss of tumor-suppressors, as well as demands of an expanding biomass contributed to tumor initiation and progression [4]. In AML, both glycolysis and oxidative phosphorylation (OxPHOS) are dysregulated and usually enhanced compared with healthy counterparts [5], and levels of glycolysis, OxPHOS, and fatty acid oxidation markedly affect proliferation and drug sensitivity of AML cells [6-9]. Understanding metabolic dependencies of cancer cells opens possibilities for targeted therapies. Such approaches include inhibiting key glycolytic enzymes, blocking nutrient transporters, or targeting altered lipid metabolism in cancer cells.

Solute carrier (SLC) transporters are mostly located in cell membrane and include over 400 members organized into 66 families [10]. These transporters are critical for maintaining cellular homeostasis, mediating the uptake and efflux of various metabolites, ions, and other molecules, including glucose, amino acids, neurotransmitters, and drugs. Recently, accumulating data showed that several SLC

family members play roles in both supporting cancer cell survival and mediating drug resistance, making them attractive targets for therapeutic intervention [11]. The mitochondrial citrate carrier SLC25A1, also known as CIC, is the transporter responsible for exporting citrate from mitochondria to cytoplasm [12, 13]. This transporter is the only known protein responsible for facilitating the exchange of citrate or isocitrate from mitochondria into cytoplasm, against malate [14]. In addition to its pivotal role in tricarboxylic acid (TCA) cycle, SLC25A1 is crucial for de novo lipogenesis and protein acetylation by regulating the levels of cytoplasmic acetyl-CoA [15, 16]. The citrate transporter SLC25A1 thus connects fatty acid metabolism with mitochondrial metabolism. SLC25A1 has been identified as an oncogene in some cancers [17-19] and dysregulation of SLC25A1 activity or expression has been associated with various diseases, where it promotes cancer cell growth and resistance to energy stress-induced apoptosis. However, the potential role of SLC25A1 in the initiation and progression of hematological malignancies through metabolic regulation, particularly AML, remains poorly understood.

In this study, we found SLC25A1 expression levels were significantly higher in AML patients. Furthermore, inhibiting SLC25A1 repressed AML cell proliferation both *in vitro* and *in vivo*, and led to mitochondrial damage and reduced fatty acid metabolism in AML cells. Overall, our findings suggest SLC25A1 could serve as a promising metabolic target for AML therapy.

Methods

Detailed descriptions of the experiments can be found in *Online Supplementary Methods.*

Ethics approval and consent to participate

The experimental protocol was approved by ethics committee of The First Hospital of China Medical University ([2022] Number174). Collection of tissue and clinicopathologic information was obtained with informed consent. Animal experiments were conducted in accordance with the China Medical University Animal Care and Use Committee guidelines and approved by the Institutional Review Board of the First Hospital of China Medical University.

Transplantation

AE9a (1×10^4) or MLL-AF9 cells (1×10^5) were injected into the tail vein of sublethally irradiated (4.75 Gy) C57BL/6N recipient mice. Survival curves, spleen weight, liver weight, and AML cell infiltration in bone marrow, spleen and peripheral blood were analyzed, respectively.

TEM

Treated Kasumi-1 and THP1 cells were harvested and fixed in TEM fixative at 4°C and pre-embedded in agarose solution. The cells were then post-fixed, dehydrated at

room temperature, resin penetrated and embedded, polymerized, and stained. The grids were finally observed and photographed in a TEM.

Mitochondrial respiratory capacity

The mitochondrial respiratory capacity was determined using an XF Cell Mito Stress Test Kit (Agilent Technologies). Cells were seeded in an XF Cell Culture Microplate and incubated for 24 h at 37°C, followed by addition of base medium containing 2 mM L-glutamine, 1 mM sodium pyruvate, and 10 mM glucose for 1 h prior to assay. The OCR was measured using an XF^e96 extracellular flux analyzer (Agilent Technologies) with sequential injection of 1.5 μM oligomycin A, 0.5 μM FCCP, and 0.5 mM rotenone/antimycin A.

RNA sequencing

Kasumi-1 cells were infected with lentivirus expressing shRNA against *SLC25A1* (scrambled shRNA as control). Cellular RNA was then extracted with TRIzol reagent (Invitrogen). An RNA-seq library was constructed using a TruSeq PE Cluster Kit v3-cBot-HS (Illumina) and sequenced with Illumina Novaseq platform. Hisat2 v2.0.5 was used to align reads to genome and featureCounts v1.5.0–p3 was used to count read numbers mapped to each gene. GO analyses were performed to analyze DEGs.

Targeted metabolomics

Targeted metabolomics was performed by Novogene Co., Ltd. (Beijing, China) to quantify selected metabolites using LC-MS/MS (SCIEX QTRAP® 6500+) in Multiple Reaction Monitoring (MRM) mode. Samples underwent targeted extraction based on metabolite properties. Method validation included assessment of linearity, precision, accuracy, and stability. Data were analyzed using standard curves generated from authentic reference compounds to ensure accurate and reproducible quantification.

Lipidomic

Kasumi-1 cells were infected with lentivirus expressing shRNA against *SLC25A1* (scrambled shRNA as control). The lipids were then extracted and subjected to UHPLC-MS/MS, as described above.

Statistical Analysis

R language (version 3.5.2) and GraphPad Prism 8 were mainly used for statistical analysis and figure drawing. Kaplan–Meier survival analysis was used to indicate prognostic values. Pearson correlation analysis was performed to test correlation of two variants. Two-tailed *t* test was performed to calculate quantitative difference between two groups. Statistical significance was defined as $P < 0.05$.

Results

SLC25A1 levels were elevated in AML

We investigated role of SLC25A1 in AML by analyzing CRISPR (DepMap 22Q2 Public+Score, Chronos) data for 26 AML cell lines. Chronos scores of SLC25A1 in most cell lines were <0, strongly suggesting that SLC25A1 was crucial in AML cells (Supplementary Figure 1A). Further analysis using GSE13159 AML database indicated a significant elevation of *SLC25A1* mRNA across different AML subtypes with specific genetic backgrounds, relative to healthy counterparts (Figure 1A). We confirmed this by using quantitative polymerase chain reaction (qPCR) analysis to analyze *SLC25A1* mRNA in AML samples from our hospital, which revealed notably higher expression in non-APL AML, compared to healthy controls (Supplementary Figure 1B). Protein levels of SLC25A1, validated by histochemistry and Western blot, were also higher in AML patients (Figure 1B and Supplementary Figure 1C) and in most human AML cell lines (Figure 1C). Additionally, data from DepMap reveals that Kasumi-1 cells and THP1 cells exhibit comparatively high levels of SLC25A1 mRNA and protein expression among AML cell lines (Supplementary Figure 1D, E). To further explore roles of SLC25A1 in leukemia stem cells (LSCs), we respectively analyzed two RNA sequencing databases of AML (GSE76009 and GSE230423) and found there was no significant difference in expression of SLC25A1 in LSCs and

blasts, indicating SLC25A1 was not a specific target in LSCs (Supplementary figure 1F). In distinct cohorts of AML patients, cases with higher *SLC25A1* expression were significantly associated with poorer outcomes (Figure 1D). Collectively, these findings underscore potential roles of SLC25A1 in the initiation and progression of AML.

SLC25A1 was crucial for the survival of AML cells

To explore the role of SLC25A1 in AML cell survival, we knocked down SLC25A1 using two different short hairpin RNAs (shRNAs; shSLC25A1-1 and shSLC25A1-2) in AML cell lines that showed high levels of SLC25A1. Both shRNAs effectively decreased expressions of SLC25A1 at both mRNA and protein levels (Supplementary Figure 2A). The knockdown (KD) of SLC25A1 significantly inhibited proliferation and clonogenicity of Kasumi-1 and THP1 cells (Figure 2A, B and Supplementary Figure 2B). Furthermore, we extended our study to primary myeloid leukemia cells, where SLC25A1 KD markedly reduced colony formation in AML#5 patient blasts (Figure 2B and Supplementary Figure 2F). To clarify mechanisms leading to the inhibition of cell proliferation, we assessed apoptosis, cell cycle, and cell differentiation in Kasumi-1 and THP1 cells, discovering that SLC25A1 KD primarily increased apoptosis without impacting cell cycle or differentiation (Figure 2C and Supplementary Figure 2C, D, E). Additionally, inhibiting SLC25A1 expression also halted proliferation of MOLM14 and OCIAML2 cell lines (Supplementary Figure

2G). These findings indicate that SLC25A1 affects AML cell survival mainly by enhancing apoptosis. HL60 cells displayed the lowest SLC25A1 levels among tested AML cell lines (Figure 1C). Notably, reducing SLC25A1 expression in HL60 cells had no impact on cell proliferation, clonogenicity, apoptosis, cell cycle, or differentiation (Supplementary Figure 3A-E). Conversely, overexpressing SLC25A1 in HL60 cells promoted cell proliferation and increased colony formation (Supplementary Figure 3F, G), yet it did not affect cell cycle or differentiation (Supplementary Figure 3H, I).

We treated Kasumi-1 and THP1 cells with the specific SLC25A1 inhibitor CTPI2, which reduced their proliferation and clonogenicity (Figure 2D and Supplementary Figure 4A). CTPI2 also inhibited growth of MOLM14 and OCIAML2 cells (Supplementary Figure 4B). CTPI2 treatment decreased viability of primary human AML cells (AML#1, AML#2, AML#4, AML#5) without affecting proliferation of healthy mononuclear cells (MNCs) (Healthy#7, Healthy#8, Healthy#9, Healthy#10) at the same concentrations (Figure 2D and Supplementary Figure 4C). Furthermore, CTPI2 treatment enhanced apoptosis in Kasumi-1 and THP1 cells (Supplementary Figure 4D).

These results suggest that SLC25A1 plays a crucial role in survival of AML cells with high SLC25A1 expression but is not essential for survival of healthy MNCs with low SLC25A1 expression.

SLC25A1 was required for the progression of AML *in vivo*

To further investigate necessity of SLC25A1 for AML maintenance and progression *in vivo*, we knock down SLC25A1 using shRNA (SLC25A1 KD) in murine AML cell lines, AE9a and MLL-AF9 (Supplementary Figure 5A). SLC25A1 KD significantly attenuated growth of these cell lines (Figure 3A). Moreover, CTPI2 markedly reduced survival of both AE9a and MLL-AF9 cells, at appropriate concentrations (Supplementary Figure 5B). Additionally, SLC25A1 KD in AE9a leukemic stem cells (LSCs) and MLL-AF9 leukemic granulocyte-macrophage progenitors (LGMPs) significantly decreased colony numbers, indicating a reduction of stemness (Figure 3B and Supplementary Figure 5C, D).

Following treatment, AE9a or MLL-AF9 cells were transplanted into sub-lethally irradiated recipient mice. The recipients of SLC25A1 KD cells exhibited extended survival (Figure 3C), smaller spleens and livers (Figure 3D and Supplementary Figure 5E), and lower percentages of leukemia blast cells (GFP^+ c-Kit^+ or GFP^+ Mac-1^-) in bone marrow, spleen, and peripheral blood (Figure 3E and Supplementary Figure 5F), compared to control mice. Histological examinations revealed fewer leukemia blasts in bone marrow and spleen of SLC25A1 KD recipients than in controls (Supplementary Figure 5G). In conclusion, these results underscore the critical role of SLC25A1 in supporting AML progression *in vivo*.

SLC25A1 deficiency compromised mitochondrial function and resulted in elevated ROS level

Given that SLC25A1 is citrate transporter on mitochondrial membrane, we investigated its impact on mitochondrial function in AML cells. After SLC25A1 KD or CTPI2 treatment, transmission electron microscopy (TEM) revealed a significant reduction in mitochondrial length, indicating structural damage (Figure 4A and Supplementary Figure 6A). Additionally, we assessed mitochondrial membrane potential using JC-1 probe via flow cytometry and fluorescence microscopy. The increased ratio of JC-1 monomers in cells with SLC25A1 KD or CTPI2 treatment suggested a decrease in mitochondrial membrane potential (Figure 4B and Supplementary Figure 6B, C). Further examination of mitochondrial function through extracellular flux analysis showed suppressed oxygen consumption rates (OCRs) in cells expressing shSLC25A1 or treated with CTPI2 (Figure 4C and Supplementary Figure 5D). These results suggest SLC25A1 deficiency impairs mitochondrial function in AML cells.

ROS are indicators of mitochondrial impairment. Consequently, we employed flow cytometry and fluorescence microscopy to measure ROS levels, confirming their increase following SLC25A1 suppression (Figure 4D and Supplementary Figure 6E, F). To assess whether ROS accumulation participated in AML cell mortality, we neutralized ROS in SLC25A1-inhibited cells using scavenger N-acetyl-L-cysteine

(NAC). The restoration of cell viability by NAC in the context of SLC25A1 inhibition suggested SLC25A1 deficiency inhibited cell survival through the upregulation of ROS (Figure 4E and Supplementary Figure 6G).

Given this, we explored the interaction between SLC25A1 inhibition and BCL-2 inhibitor venetoclax, which suppresses cell growth partly through ROS induction [20, 21]. Treatment of AML cells with venetoclax in SLC25A1 KD group resulted in heightened drug sensitivity compared to the control (Supplementary Figure 7A). Furthermore, addition of CTPI2 to treatments with venetoclax led to a synergistic suppression of AML cell growth (Supplementary Figure 7B). We also detected the effect on cell apoptosis by flow cytometry and found ratio of apoptotic cells was significantly increased in cells treated with CTPI2 plus venetoclax (Supplementary Figure 7C). An examination of ROS levels across control, single treatment, and combination treatment groups demonstrated the combination yielded the highest ROS levels (Supplementary Figure 7D). Collectively, these results indicate the potential of SLC25A1 inhibitor CTPI2 to enhance sensitivity of ROS-generating drugs like venetoclax by synergistically enhancing ROS-induced apoptosis.

Deletion of SLC25A1 disrupted fatty acid metabolism

To investigate deeper mechanism of SLC25A1 in AML, we analyzed SLC25A1-related genes (R>0.5) within The Cancer Genome Atlas (TCGA) and Vizome AML databases [22] using Gene Ontology (GO), revealing a substantial

metabolic association in nearly half of identified GO terms (Supplementary Figure 8A, B). We also performed RNA sequencing analysis of control and SLC25A1 KD AML cells. GO analysis of differentially expressed genes (DEGs) and GSEA showed SLC25A1 was closely correlated with ROS metabolic process, extrinsic apoptotic signaling pathway and oxidative phosphorylation (Supplementary Figure 8C). Besides the above pathways, we also found that metabolic pathways, including nicotinate metabolism and fatty acid metabolism, were enriched by analyzing DEGs (Supplementary Figure 8C). We further analyzed differences in metabolites between the control and SLC25A1 KD groups by metabolomics, finding that a series of fatty acid metabolism pathways were enriched, including alpha linolenic acid and linoleic acid metabolism, biosynthesis of unsaturated fatty acids, carnitine synthesis and transfer of acetyl groups into mitochondria (Figure 5A). Moreover, fatty acid homeostasis was enriched in SLC25A1-high group (Supplementary Figure 8D).

Combining GO analysis of RNA sequencing and metabolomics, we focused on changes in fatty acid metabolism (fatty acid oxidation and fatty acid synthesis) following SLC25A1 KD and identified four genes (*CPT1A*, *CPT1C*, *ACLY*, and *FASN*) downregulated in RNA sequencing that are intimately connected to fatty acid metabolism (Figure 5B). Protein interaction network analysis via STRING and GeneMANIA online tools further implicated SLC25A1 in associations with enzymes of fatty acid synthesis (ACLY and FASN) (Supplementary Figure 8E, F). Additionally, positive correlation between *SLC25A1* expression and levels of enzymes in AML

databases was validated (Supplementary Figure 8G, H). Protein expression levels of CPT1A, CPT1C, ACLY, and FASN in Kasumi-1 and THP1 cells decreased after SLC25A1 KD (Figure 5C and Supplementary Figure 8I, J). Based on changes in expression levels of key enzymes in fatty acid metabolism, we looked for related metabolite changes through metabolomics data. Citrate in mitochondria, the substrate of SLC25A1, was increased after SLC25A1 KD, while coenzyme A, the product of ACLY from citrate and the substrate of fatty acid synthesis, decreased after SLC25A1 KD (Supplementary Figure 8K, L), leading to TCA cycle overloading, elevated ROS levels, and changes in fatty acid metabolites. Meanwhile, supplementation with citrate in cytoplasm of SLC25A1 KD cells can restore expression of ACLY and FASN (Figure 5C), indicating direct regulation of SLC25A1 on ACLY and FASN through citrate. Considering the significance of fatty acid oxidation, where carnitine serves as a shuttle for fatty acids into mitochondria, we observed diminished levels of five carnitine-related intermediates (L-carnitine, palmitoylcarnitine, acetyl-carnitine, propionylcarnitine, hexanoylcarnitine) produced by carnitine acyl transferases CPT1A and CPT1C following SLC25A1 KD (Figure 5D). Lipidomic assessment revealed a reduction in palmitic acid, a vital long-chain fatty acid synthesized by FASN, in SLC25A1 KD group, and extra supplementation with palmitic acid in SLC25A1 KD cells rescued the proliferation defect and restored the reduced oxygen consumption rate (OCR) caused by the knockdown (Figure 5E and Supplementary Figure 8M).

Together, these results suggest SLC25A1 deletion reduces fatty acid oxidation and synthesis.

In-depth lipidomic analysis revealed most phosphoglycerides (PGs) and triglycerides (TAGs) were elevated after SLC25A1 KD (Figure 5F and Supplementary Figure 8N). The lipids play cytoprotective roles by forming lipid droplets [23], suggesting that the effect might involve a self-protection mechanism after stress. DGAT1, a key enzyme catalyzing conversion of fatty acids to TAGs [24], was found to be upregulated in protein expression level after SLC25A1 KD (Figure 5F and Supplementary Figure 8O). When AML cells underwent treatment with a DGAT1 inhibitor, A922500 [25] in combination with CTPI2, a notable synergistic effect was observed (Figure 5F and Supplementary Figure 8P). These results reveal SLC25A1 deletion initiates self-protection by increasing PGs and TAGs which can be reversed by inhibiting DGAT1.

A novel SLC25A1 inhibitor CTPI3 showed high effectiveness and safety, synergizing with venetoclax

Given the relatively high working concentration required for CTPI2 in AML cell lines, we sought to identify a more specific and potent inhibitor of SLC25A1. We screened FDA-approved drug library based on “Fit Value” scores and selected compounds with Fit Value > 1 for further structural optimization. Using Induced Fit Docking (IFD) module in the Schrödinger Suite, flexible molecular docking of candidate compounds was performed against active site of SLC25A1. This approach led to the identification

of a new-generation inhibitor, CTPI3, with an improved predicted binding conformation (Figure 6A). CTPI3 significantly reduced the viability of primary AML cells, Kasumi-1, THP1, AE9a, and MLL-AF9, while showing less toxicity towards healthy MNCs (Figure 6B). CTPI3 induced apoptosis in Kasumi-1 and THP1 cells (Supplementary Figure 9A). In both AE9a and MLL-AF9 murine leukemia models, CTPI3 treatment extended overall survival compared to vehicle controls (Figure 6C). *In vivo*, CTPI3 led to notable reductions in spleen size, less disruption of splenic architecture, and decreased $GFP^{+}Mac\text{-}1^{-}$ cell populations in bone marrow, spleen, and peripheral blood (Figure 6D and Supplementary Figure 9B). The treatment group exhibited higher hemoglobin and platelet counts (Supplementary Figure 9C). Body weight remained stable during treatment, and H&E staining as well as c-caspase 3 immunohistochemical staining of liver, kidney, and brain showed no significant toxicity (Figure 6E and Supplementary Figure 9C). These results indicate CTPI3 we newly developed potently inhibits AML cells growth *in vitro and in vivo*, with no obvious toxicity.

Following CTPI3 treatment, TCA metabolites (α-ketoglutarate, pyruvic acid, oxalic acid, fumaric acid, maleic acid, and succinic acid) were all reduced (Supplementary Figure 10A), which was accord with results in Figure 4. Moreover, combining CTPI3 with venetoclax resulted in high synergistic anti-leukemic effects, including enhanced suppression of proliferation and ATP production (Figure 6F). Meanwhile, targeted metabolomics revealed a marked reduction in both TCA cycle intermediates and fatty

acids following combined treatment, with significant reduction of CPT1A and CPT1C expression (Figure 6F and Supplementary Figure 10B, C). The outcomes reveal targeting SLC25A1 by CTPI3 effectively improves sensitivity of venetoclax through inhibiting fatty acid metabolism.

Discussion

The poor prognosis and resistance to existing pharmacotherapies for many AML patients leads to an urgent need for new therapeutic targets. Recently, accumulating data showed dysregulated cellular metabolism is one of hallmarks of tumor and plays important roles in tumor growth, progression and drug resistance [26-28]. Citrate, an essential metabolite in both mitochondria and cytoplasm, regulates cellular energy homeostasis in tumors [29]. Here, we show citrate transporter SLC25A1, a clinical biomarker for AML patients, is required for survival of leukemic cells, both *in vitro* and *in vivo*. Depletion of SLC25A1 promotes ROS-induced apoptosis by impairing mitochondrial function through TCA cycle. Inhibition of SLC25A1 could enhance sensitivities of AML cells to venetoclax. Mechanistic studies show citrate homeostasis disturbance significantly suppresses growth of AML cells accompanied by affecting fatty acid metabolism. These findings suggest SLC25A1 plays a pivotal role in AML and represents a potential novel therapeutic target (Figure 7).

Previous studies revealed SLC25A1 acted as an oncogene in the progression of solid tumors [17-19, 30, 31], yet its molecular mechanism has not been fully elucidated and its role in AML remains unclear [32]. Our data shows SLC25A1 is a clinically significant biomarker highly expressed in patients with different subtypes of AML which is correlated with inferior prognosis in patients. Interestingly, suppressing SLC25A1 significantly inhibited growth of both AML cell lines and primary cells from AML patients, but had no effect on normal MNCs. Moreover, knockdown of SLC25A1 blocked the progression of AML *in vivo*. These findings collectively indicate SLC25A1 plays an important role in the promotion of AML and could serve as a therapeutic target for suppression of AML cell growth. We confirmed at cellular level that SLC25A1 inhibitor CTPI2 can effectively inhibit survival of AML cells, but the effective concentration of this inhibitor is relatively high, making it unsuitable for drug treatment exploration in mouse models. To improve clinical value of SLC25A1 targeting therapy, we synthesized new generation of SLC25A1 inhibitors based on structure of CTPI2. We named it as CTPI3. CTPI3 showed higher sensitivity in both AML cell lines and primary AML cells from patients, but had no toxicity in healthy MNCs with the same concentration. More significantly, CTPI3 application *in vivo* expanded survival of AML mice and decreased infiltration of AML cells in bone marrow, spleen and peripheral blood, without obvious toxicity in important organs. CTPI3 developed by our team might extremely promote SLC25A1 targeting therapy in future.

Metabolic reprogramming is an important tumor characteristic. In recent years, increasing evidence has shown besides glucose metabolism and oxidative phosphorylation, amino acid metabolism and fatty acid metabolism also play important roles in tumorigenesis and drug resistance [33-36]. Here we found inhibiting SLC25A1 damaged mitochondrial function and affected the growth of AML cells by promoting ROS induced apoptosis, without affecting the cell cycle and differentiation. Mitochondria are the central hub for oxidative phosphorylation and fatty acid metabolism [37]. Indeed, we found SLC25A1 depletion disturbs fatty acid metabolism. Intriguingly, a series of important enzymes involved in fatty acid synthesis and oxidation are downregulated upon SLC25A1 blockage, including ACLY, FASN, CPT1A, and CPT1C. We verified the regulation of SLC25A1 on FA enzymes through citrate rescue experiment. We also confirmed the important role of palmitic acid in cell growth and oxidative phosphorylation by palmitic acid addition. Based on current evidence, we speculate that the downregulation of enzymes involved in fatty acid synthesis and oxidation is most likely an adaptive cellular response to the metabolic crisis caused by SLC25A1 deficiency, rather than a result of direct molecular interactions. However, whether SLC25A1 can directly interact with and regulate transcription factors such as MYC or SREBP1, which govern the expression of many enzymes involved in fatty acid metabolism, remains to be further explored. Mitochondrial metabolism and fatty acid metabolism are essential for cell energy supplementation, with important roles in the initiation and progression of AML [26, 38].

Our results indicate that singly targeting SLC25A1 might effectively kill AML cells through simultaneously affecting multiple metabolic pathways including mitochondrial metabolism and fatty acid metabolism.

DGAT1, a key enzyme catalyzing conversion of fatty acids to TAGs, is found to be upregulated. Lipid droplets formed by TAGs and PGs may protect cells from oxidative stress [23, 39]. Cells initiate self-protective mechanisms by upregulating DGAT1 expression, producing more TAGs and PGs to provide alternative energy compensation and inhibit apoptosis, potentially contributing to cellular resistance mechanisms. Inhibiting DGAT1 can enhance AML cells' sensitivity to SLC25A1 inhibition, providing a new direction for improving the efficiency of SLC25A1-targeted therapies. SLC25A1 was previously shown to regulate metabolites in fatty acid metabolism in solid tumors [17, 19, 40] and our current study has extended these findings, contributing to more detailed molecular mechanism.

The targeted drug venetoclax is first-line therapy in older AML, inducing apoptosis in AML cells by inhibiting BCL2 [41, 42]. However, besides classic mechanism, recent studies revealed venetoclax inhibited mitochondrial metabolism to induce cell death [6, 43], yet resistance and recurrence persist as significant challenges [42, 44-46]. Up-regulation of fatty acid oxidation (FAO) compensates the inhibition of amino acid metabolism by venetoclax, leading to venetoclax resistance [47]. But FAO direct inhibitor might have toxicity on other important organs, without clinical significance. Of note, a

recent study identified SLC25A1 as a significant gene influencing venetoclax sensitivity through CRISPR screening [1], which indicated targeting SLC25A1 might overcome the resistance of venetoclax. Our novel findings showed that SLC25A1 inhibitor, CTPI3 could synergistically target AML cells with venetoclax by inhibiting mitochondrial and fatty acid metabolism. As SLC25A1 was only high expressed in AML cells, targeting SLC25A1 might be safer than FAO inhibitor to improve sensitivity of venetoclax, which provides high clinical value.

Our study firstly demonstrates metabolic reprogramming induced by SLC25A1 in AML, which leads to the progression of AML as well as venetoclax resistance of patients. These findings improve our cognition in the roles of metabolic regulation in AML development and treatment, providing the basis of personalized therapy targeted on metabolism disorder. In conclusion, targeting mitochondrial metabolism and fatty acid metabolism using SLC25A1 inhibitor might be a potential novel strategy for enhancing AML therapy and overcoming drug resistance.

List of abbreviations

AML: Acute myeloid leukemia
OxPHOS: oxidative phosphorylation
SLC: Solute carrier
TCA: tricarboxylic acid
qPCR: quantitative polymerase chain reaction
KD: knockdown
MNCs: mononuclear cells
LSCs: leukemic stem cells
LGMPs: leukemic granulocyte-macrophage progenitors
TEM: transmission electron microscopy

OCRs: oxygen consumption rates
NAC: N-acetyl-L-cysteine
DNR: daunorubicin
TCGA: The Cancer Genome Atlas
GO: Gene Ontology
DEGs: differentially expressed genes
PGs: phosphoglycerides
TAGs: triglycerides

References

1. Chen X, Glytsou C, Zhou H, et al. Targeting Mitochondrial Structure Sensitizes Acute Myeloid Leukemia to Venetoclax Treatment. Cancer Discov. 2019;9(7):890-909.

2. MacPherson L, Anokye J, Yeung M, et al. HBO1 is required for the maintenance of leukaemia stem cells. Nature. 2020;577(7789):266-270.

3. Miller K, Nogueira L, Mariotto A, et al. Cancer treatment and survivorship statistics, 2019. CA Cancer J Clin. 2019;69(5):363-385.

4. Vander Heiden MG, DeBerardinis RJ. Understanding the Intersections between Metabolism and Cancer Biology. Cell. 2017;168(4):657-669.

5. DeBerardinis RJ, Chandel NS. We need to talk about the Warburg effect. Nat Metab. 2020;2(2):127-129.

6. Sharon D, Cathelin S, Mirali S, et al. Inhibition of mitochondrial translation overcomes venetoclax resistance in AML through activation of the integrated stress response. Sci Transl Med. 2019;11(516):eaax2863.

7. Skrtić M, Sriskanthadevan S, Jhas B, et al. Inhibition of mitochondrial translation as a therapeutic strategy for human acute myeloid leukemia. Cancer Cell. 2011;20(5):674-688.

8. Farge T, Saland E, de Toni F, et al. Chemotherapy-Resistant Human Acute Myeloid Leukemia Cells Are Not Enriched for Leukemic Stem Cells but Require Oxidative Metabolism. Cancer Discov. 2017;7(7):716-735.

9. Samudio I, Harmancey R, Fiegl M, et al. Pharmacologic inhibition of fatty acid oxidation sensitizes human leukemia cells to apoptosis induction. J Clin Invest. 2010;120(1):142-156.

10. Perland E, Fredriksson R. Classification Systems of Secondary Active Transporters. Trends Pharmacol Sci. 2017;38(3):305-315.

11. Elena P, Gert F, Mikko G. The Role of Solute Carrier Transporters in Efficient Anticancer Drug Delivery and Therapy. Pharmaceutics. 2023;15(2):364.

12. Palmieri F, Monné M. Discoveries, metabolic roles and diseases of mitochondrial carriers: A review. Biochim Biophys Acta. 2016;1863(10):2362-2378.

13. Palmieri F. Mitochondrial transporters of the SLC25 family and associated diseases: a review. J Inherit Metab Dis. 2014;37(4):565-575.

14. Palmieri F. The mitochondrial transporter family SLC25: identification, properties and physiopathology. Mol Aspects Med. 2013;34(2-3):465-484.

15. Ma C, Gerhard E, Lu D, Yang J. Citrate chemistry and biology for biomaterials design. Biomaterials. 2018;178:383-400.

16. Zhang Z, Qiao Y, Sun Q, Peng L, Sun L. A novel SLC25A1 inhibitor, parthenolide, suppresses the growth and stemness of liver cancer stem cells with metabolic vulnerability. Cell Death Discov. 2023;9(1):350.

17. Fernandez HR, Gadre SM, Tan M, et al. The mitochondrial citrate carrier, SLC25A1, drives stemness and therapy resistance in non-small cell lung cancer. Cell Death Differ. 2018;25(7):1239-1258.

18. Ozkaya AB, Ak H, Atay S, Aydin HH. Targeting mitochondrial citrate transport in breast cancer cell lines. Anticancer Agents Med Chem. 2015;15(3):374-381.

19. Yang Y, He J, Zhang B, et al. SLC25A1 promotes tumor growth and survival by reprogramming energy metabolism in colorectal cancer. Cell Death Dis. 2021;12(12):1108.

20. Lee J, Khan D, Hurren R, et al. Venetoclax enhances T cell-mediated antileukemic activity by increasing ROS production. Blood. 2021;138(3):234-245.

21. Chiou J, Huang N, Huang C, et al. NOXA-mediated degradation of MCL1 and BCL2L1 causes apoptosis of daunorubicin-treated human acute myeloid leukemia cells. J Cell Physiol. 2021;236(11):7356-7375.

22. Tyner J, Tognon C, Bottomly D, et al. Functional genomic landscape of acute myeloid leukaemia. Nature. 2018;562(7728):526-531.

23. Olzmann J, Carvalho P. Dynamics and functions of lipid droplets. Nature reviews Mol Cell Biol. 2019;20(3):137-155.

24. Dias S, Soares V, Ferreira A, et al. Lipid droplets fuel SARS-CoV-2 replication and production of inflammatory mediators. PLoS Pathog. 2020;16(12):e1009127.

25. Zhou J, Simon J, Liao C, et al. An oncogenic JMJD6-DGAT1 axis tunes the epigenetic regulation of lipid droplet formation in clear cell renal cell carcinoma. Mol Cell. 2022;82(16):3030-3044.e8.

26. Mishra S, Millman S, Zhang L. Metabolism in acute myeloid leukemia: mechanistic insights and therapeutic targets. Blood. 2023;141(10):1119-1135.

27. Egan G, Schimmer A. Contribution of metabolic abnormalities to acute myeloid leukemia pathogenesis. Trends Cell Biol. 2023;33(6):455-462.

28. Hanahan D. Hallmarks of Cancer: New Dimensions. Cancer Discov. 2022;12(1):31-46.

29. Yangjing Z, Xia L, Fusheng S, et al. Citrate Promotes Excessive Lipid Biosynthesis and Senescence in Tumor Cells for Tumor Therapy. Adv Sci (Weinh). 2021;9(1):e2101553.

30. Mosaoa R, Kasprzyk-Pawelec A, Fernandez H, Avantaggiati M. The Mitochondrial Citrate Carrier SLC25A1/CIC and the Fundamental Role of Citrate in Cancer, Inflammation and Beyond. Biomolecules. 2021;11(2):141.

31. Hlouschek J, Hansel C, Jendrossek V, Matschke J. The Mitochondrial Citrate Carrier (SLC25A1) Sustains Redox Homeostasis and Mitochondrial Metabolism Supporting Radioresistance of Cancer Cells With Tolerance to Cycling Severe Hypoxia. Front Oncol. 2018;8:170.

32. Liu F, Deng S, Li Y, Du J, Zeng H. SLC25A1-associated prognostic signature predicts poor survival in acute myeloid leukemia patients. Front Genet. 2022;13:1081262.

33. Lee K, Giltnane J, Balko J, et al. MYC and MCL1 Cooperatively Promote Chemotherapy-Resistant Breast Cancer Stem Cells via Regulation of Mitochondrial Oxidative Phosphorylation. Cell Metab. 2017;26(4):633-647.e7.

34. Hattori A, Tsunoda M, Konuma T, et al. Cancer progression by reprogrammed

BCAA metabolism in myeloid leukaemia. Nature. 2017;545(7655):500-504.

35. Ye H, Adane B, Khan N, et al. Leukemic Stem Cells Evade Chemotherapy by Metabolic Adaptation to an Adipose Tissue Niche. Cell stem cell. 2016;19(1):23-37.

36. Martínez-Reyes I, Chandel N. Cancer metabolism: looking forward. Nat Rev Cancer. 2021;21(10):669-680.

37. Yashi M, Guoyuan Q, Francesca V, et al. Loss of fatty acid degradation by astrocytic mitochondria triggers neuroinflammation and neurodegeneration. Nat Metab. 2023;5(3):445-465.

38. Shao X, Xu A, Du W, et al. The palmitoyltransferase ZDHHC21 regulates oxidative phosphorylation to induce differentiation block and stemness in AML. Blood. 2023;142(4):365-381.

39. Lee S, Li J, Tai J, Ratliff T, Park K, Cheng J. Avasimibe encapsulated in human serum albumin blocks cholesterol esterification for selective cancer treatment. ACS Nano. 2015;9(3):2420-2432.

40. Zhang R, Peng X, Du J, et al. Oncogenic KRASG12D Reprograms Lipid Metabolism by Upregulating SLC25A1 to Drive Pancreatic Tumorigenesis. Cancer Res. 2023;83(22):3739-3752.

41. Chan S, Thomas D, Corces-Zimmerman M, et al. Isocitrate dehydrogenase 1 and 2 mutations induce BCL-2 dependence in acute myeloid leukemia. Nat Med. 2015;21(2):178-184.

42. DiNardo C, Tiong I, Quaglieri A, et al. Molecular patterns of response and

treatment failure after frontline venetoclax combinations in older patients with AML. Blood. 2020;135(11):791-803.

43. Jones C, Stevens B, D'Alessandro A, et al. Inhibition of Amino Acid Metabolism Selectively Targets Human Leukemia Stem Cells. Cancer Cell. 2018;34(5):724-740.e4.

44. Thomalla D, Beckmann L, Grimm C, et al. Deregulation and epigenetic modification of BCL2-family genes cause resistance to venetoclax in hematologic malignancies. Blood. 2022;140(20):2113-2126.

45. Li X, Xu S, Tan Y, Chen J. The effects of idarubicin versus other anthracyclines for induction therapy of patients with newly diagnosed leukaemia. Cochrane Database Syst Rev. 2015;2015(6):CD010432.

46. Zhang X, Yang L, Liu X, et al. Regulatory role of RBM39 in acute myeloid leukemia: Mediation through the PI3K/AKT pathway. Biochimica et biophysica acta Mol Cell Res. 2024;1871(1):119607.

47. Stevens B, Jones C, Pollyea D, et al. Fatty acid metabolism underlies venetoclax resistance in acute myeloid leukemia stem cells. Nat Cancer. 2020;1(12):1176-1187.

Figures Legends

Figure 1. SLC25A1 is highly expressed in AML. (A) The mRNA expression of SLC25A1 in healthy donors (n=74) and AML patients (n=542) in GSE13159 database; mRNA expression of SLC25A1 in healthy donors (n=74) and AML patients of various subtypes, including t(8:21) (n=40), t(11q23) (n=38), inv(16)/t(16:16) (n=28), Normal karyotype (n=351) and Complex aberrant karyotype (n=48) in GSE13159 database. (B) The immunohistochemistry analysis of SLC25A1 protein expression in BM mononuclear cells from healthy donors (n=3) and AML patients (n=3). (C) The western blotting analysis of SLC25A1 expression in healthy donors and various patient-derived AML cell lines. (D) The survival analysis of SLC25A1 in two AML databases (Log-rank test).

Figure 2. SLC25A1 is required for survival of AML cells in vitro. (A) The growth of Kasumi-1 and THP1 cells was inhibited after SLC25A1 knockdown with shControl, shSLC25A1-1 and shSLC25A1-2 lentiviruses. (B) The colony formation assay of Kasumi-1, THP1 cells and human primary AML cells (AML#5) after SLC25A1 knockdown with shControl, shSLC25A1-1 and shSLC25A1-2 lentiviruses. (C) The percentage of apoptotic leukemia cells at day 2 after SLC25A1 knockdown. (D) The growth of Kasumi-1 and THP1 cells was inhibited after SLC25A1 inhibitor (CTPI2) application. The growth of human primary AML cells (AML#1, #2, #4, #5) cells was

inhibited after CTPI2 application, but the growth of mononuclear cells from healthy bone marrow (Healthy#7, #8, #9, #10) was not affected.

Figure 3. SLC25A1 is required for survival of AML cells *in vivo*. (A) The growth of AE9a cells and MLL-AF9 cells was inhibited after SLC25A1 knockdown with shControl, shSLC25A1-1 and shSLC25A1-2 lentiviruses. (B) The colony formation assay of AE9a LSCs and MLL-AF9 LGMPs after SLC25A1 knockdown. (C) Kaplan-Meier survival curves of recipient mice transplanted with AE9a cells and MLL-AF9 cells after SLC25A1 knockdown. A log-rank test was performed. (D) The weight changes of the spleen in recipient mice transplanted with AE9a cells after SLC25A1 knockdown. (E) The frequencies of $GFP^+c\text{-}Kit^+$ or GFP^+Mac1^-leukemia blast cells in the bone marrow and the spleen of recipient mice transplanted with shControl AE9a cells and shSLC25A1 AE9a cells.

Figure 4. SLC25A1 affects the function of mitochondria and the cellular ROS level. (A) The change of mitochondrial length under transmission electron microscope after SLC25A1 knockdown and CTPI2 application in Kasumi-1. (B) The change of mitochondrial membrane potential through flow cytometry after SLC25A1 knockdown and CTPI2 application in Kasumi-1. (C) The OCRs measured by seahorse extracellular flux analyzer experiment after SLC25A1 knockdown and CTPI2 application in Kasumi-1. (D) The cellular ROS levels measured by flow cytometry after SLC25A1

knockdown and CTPI2 application in Kasumi-1. (E) The growth of Kasumi-1 cells after SLC25A1 knockdown and CTPI2 application is rescued by ROS remover (NAC).

Figure 5. Knockdown of SLC25A1 inhibits fatty acid metabolism and initiates self-protection of AML cells. (A) The GO enrichment analysis of differential metabolites performed by metabolomics on Kasumi-1 with SLC25A1 knockdown. (B) The volcano plot of DEGs performed by RNA sequencing on Kasumi-1 with SLC25A1 knockdown. (C) The WB validation of SLC25A1 KD on the expression of ACLY and FASN in Kasumi-1 cells (left panel). The WB validation of ACLY and FASN expression following SLC25A1 KD and citrate supplementation (right panel). (D) The heat map showing the change of carnitine related metabolites (palnitoylcarnitine, propionylcarnitine, hexanoylcarnitine, L (-)-carnitine and acetyl-L-carnitine) level detected by metabolomics after SLC25A1 knockdown in Kasumi-1 cells. (E) The change of palmitic acid level detected by lipidomics after SLC25A1 knockdown in Kasumi-1 cells (left panel). Palmitic acid supplementation partially rescues impaired mitochondrial function in SLC25A1 KD cells (right panel). (F) The heat map showing the change of TAG level detected by lipidomics after SLC25A1 knockdown in Kasumi-1 cells (left panel). The validation of DGAT1 expression by WB after SLC25A1 knockdown in Kasumi-1 (middle panel). The synergistic effect of CTPI2 and DGAT1i (A922500) on inhibiting the growth of Kasumi-1 (right panel).

Figure 6. CTPI3 inhibits AML cell viability and synergizes with venetoclax *in vitro,* as well as inhibits AML progression *in vivo*. (A) Predicted binding mode of CTPI3 to the active site of SLC25A1 based on molecular docking analysis. (B) Dose–response curves showing the inhibitory effects of CTPI3 on AML cell lines (Kasumi-1, THP1, AE9a, MLL-AF9), primary AML blasts, and healthy mononuclear cells (MNCs). (C) Kaplan–Meier survival curves of mice bearing AE9a (left panel) or MLL-AF9 (right panel) AML models treated with CTPI3 (n = 7 per group). (D) *In vivo* efficacy of CTPI3 in the AE9a model: reduction in GFP^$^{+}$Mac-1^$^{-}$ leukemia burden in bone marrow (BM), spleen (SP) compared to control mice. (E) Body weight monitoring post-CTPI3 treatment. (F) CTPI3 sensitizes AML cells to venetoclax. Left: Cell viability in Kasumi-1 cells treated with venetoclax and CTPI3. Middle: Mitochondrial ATP production is reduced upon CTPI3 or combination treatment. Right: Heatmap showing altered levels of key TCA intermediates and fatty acids following combination treatment.

Figure 7. The work mechanism of SLC25A1 in AML cells.

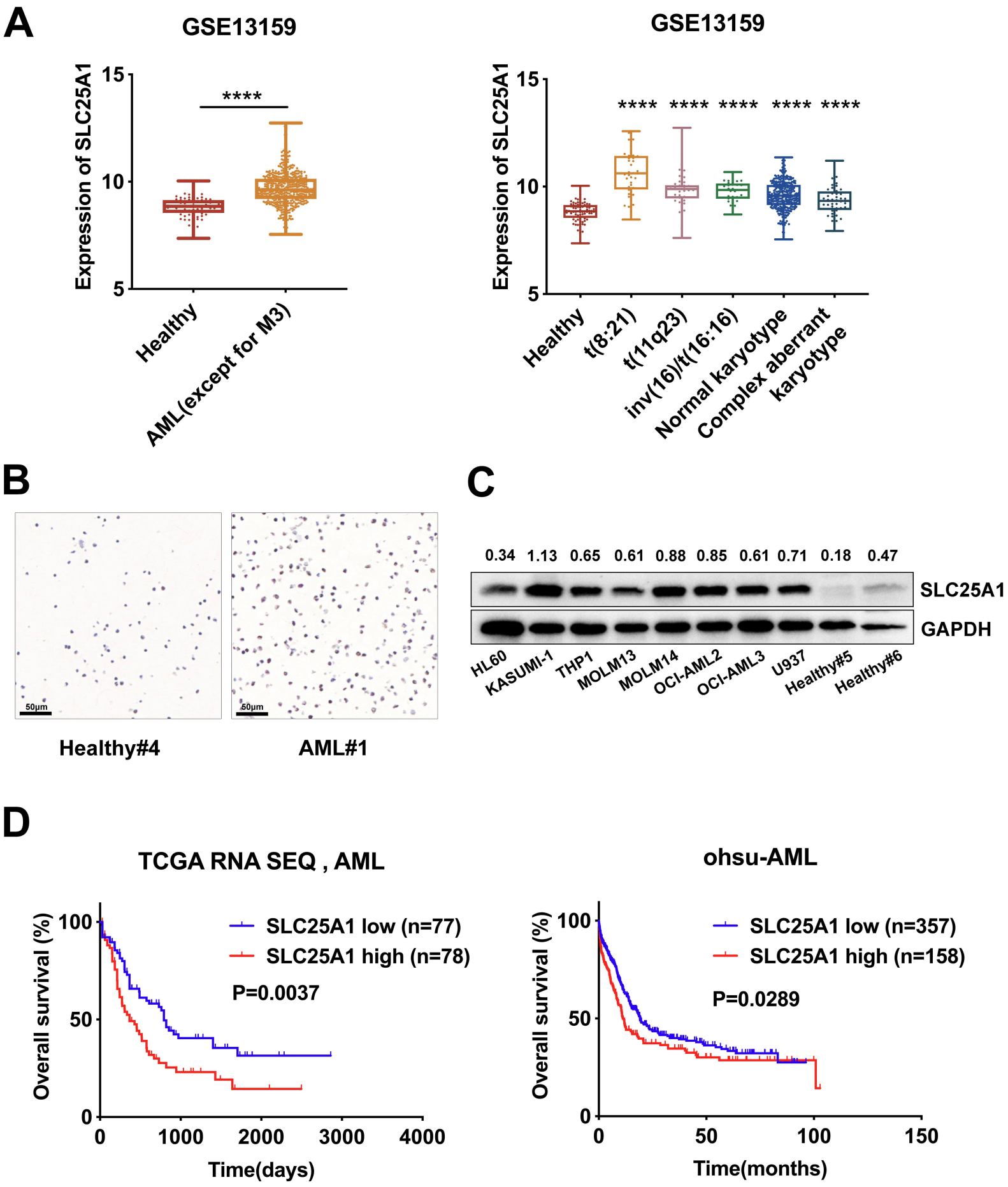
A
GSE13159
Expression of SLC25A1
15
10
5
****
Healthy
AML(except for M3)
GSE13159
Expression of SLC25A1
15
10
5
**** **** **** **** ****
Healthy
t(8:21)
t(11q23)
inv(16)/t(16:16)
Normal karyotype
Complex aberrant karyotype
B
50μm
50μm
Healthy#4
AML#1
C
0.34 1.13 0.65 0.61 0.88 0.85 0.61 0.71 0.18 0.47
SLC25A1
GAPDH
HL60
KASUMI-1
THP1
MOLM13
MOLM14
OCI-AML2
OCI-AML3
U937
Healthy#5
Healthy#6
D
TCGA RNA SEQ , AML
Overall survival (%)
100
50
0
SLC25A1 low (n=77)
SLC25A1 high (n=78)
P=0.0037
0
1000
2000
3000
4000
Time(days)
ohsu-AML
Overall survival (%)
100
50
0
SLC25A1 low (n=357)
SLC25A1 high (n=158)
P=0.0289
0
50
100
150
Time(months)

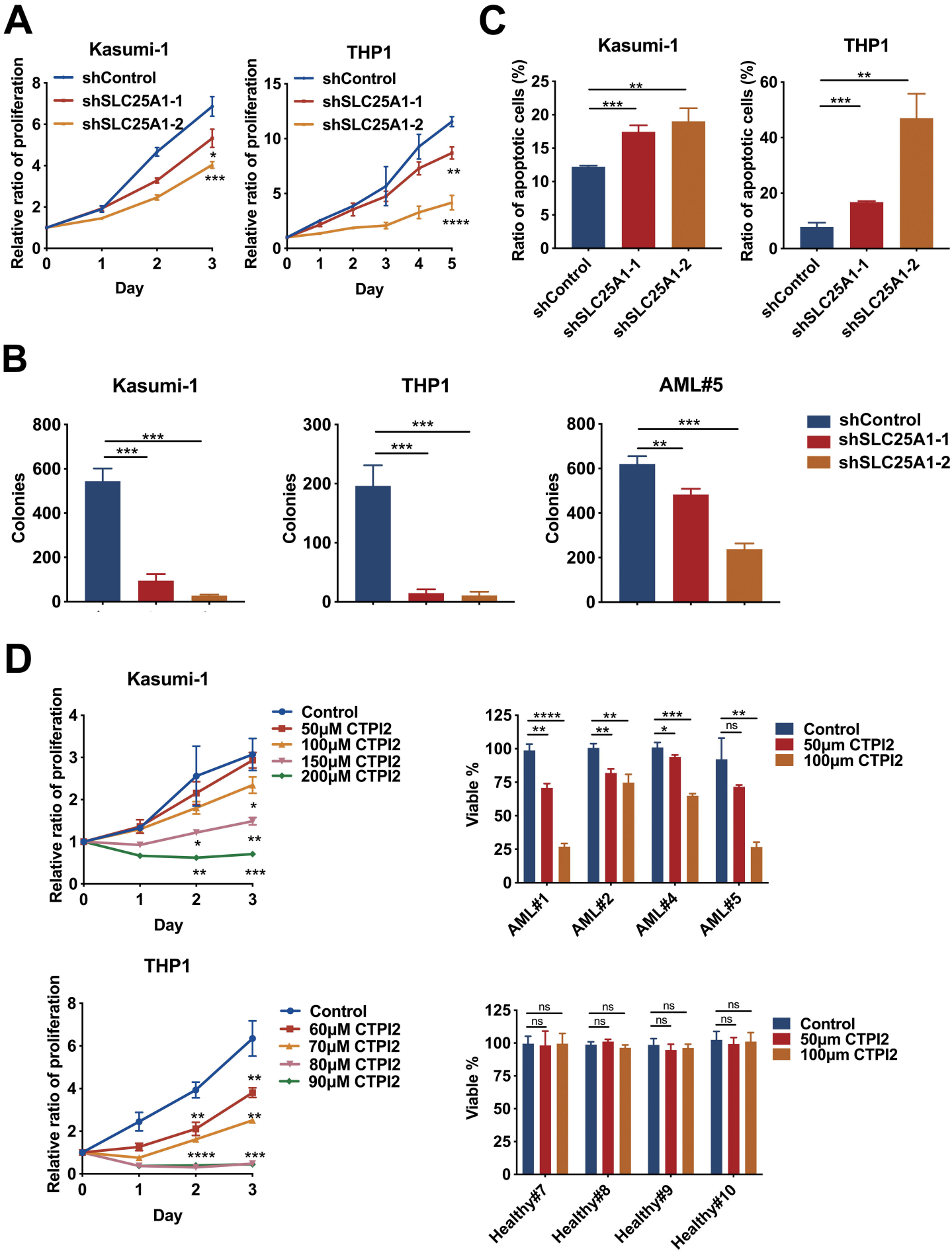
A
Kasumi-1
shControl
shSLC25A1-1
shSLC25A1-2
Relative ratio of proliferation
Day
THP1
C
Ratio of apoptotic cells (%)
B
Colonies
AML#5
D
Control
50μM CTPI2
100μM CTPI2
150μM CTPI2
200μM CTPI2
60μM CTPI2
70μM CTPI2
80μM CTPI2
90μM CTPI2
Viable %
50μm CTPI2
100μm CTPI2
AML#1
AML#2
AML#4
AML#5
Healthy#7
Healthy#8
Healthy#9
Healthy#10
ns

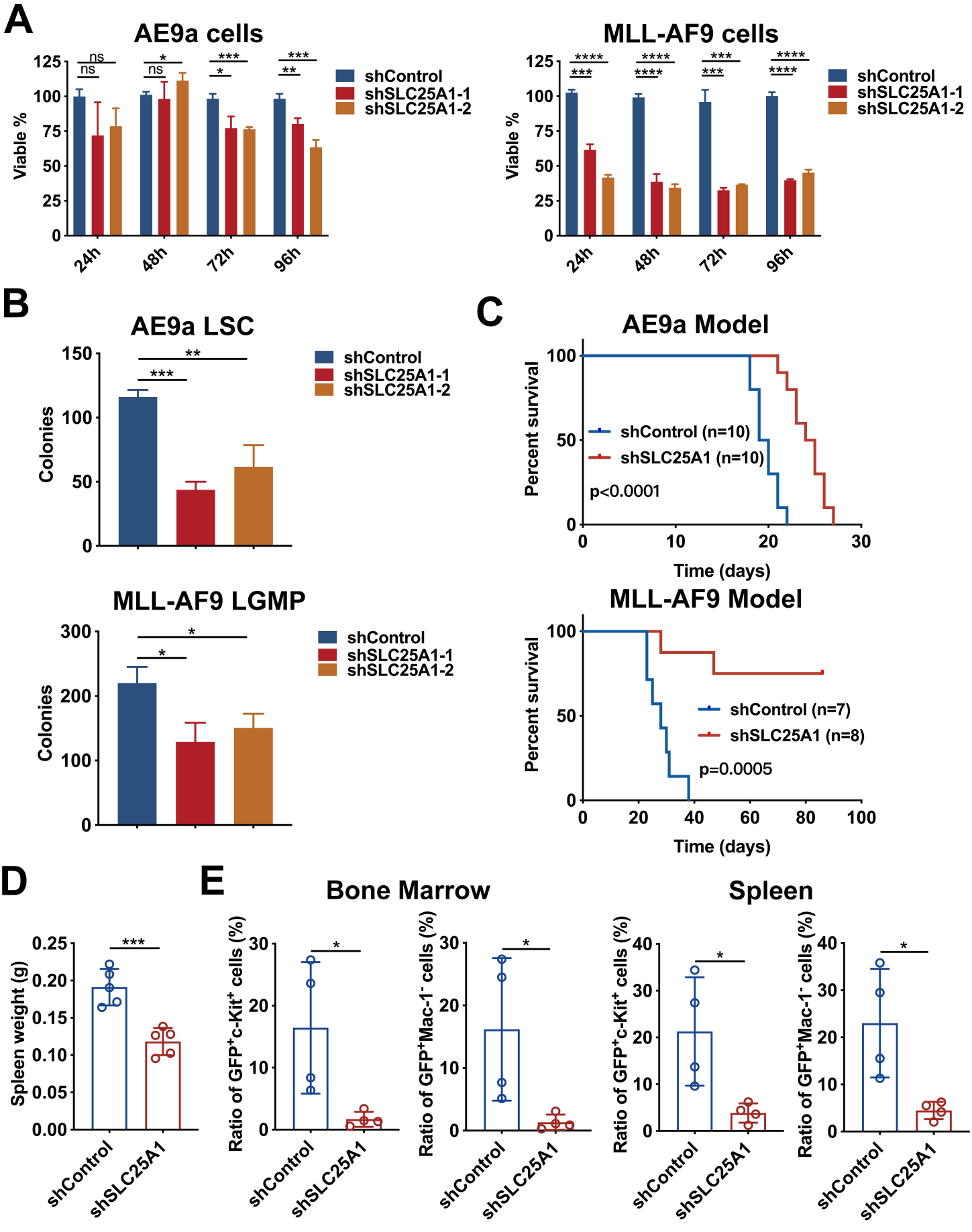
A
AE9a cells
Viable %
shControl
shSLC25A1-1
shSLC25A1-2
24h
48h
72h
96h
MLL-AF9 cells
B
AE9a LSC
Colonies
MLL-AF9 LGMP
C
AE9a Model
Percent survival
shControl (n=10)
shSLC25A1 (n=10)
p<0.0001
Time (days)
MLL-AF9 Model
shControl (n=7)
shSLC25A1 (n=8)
p=0.0005
D
Spleen weight (g)
shControl
shSLC25A1
E
Bone Marrow
Spleen
Ratio of GFP+c-Kit+ cells (%)
Ratio of GFP+Mac-1- cells (%)

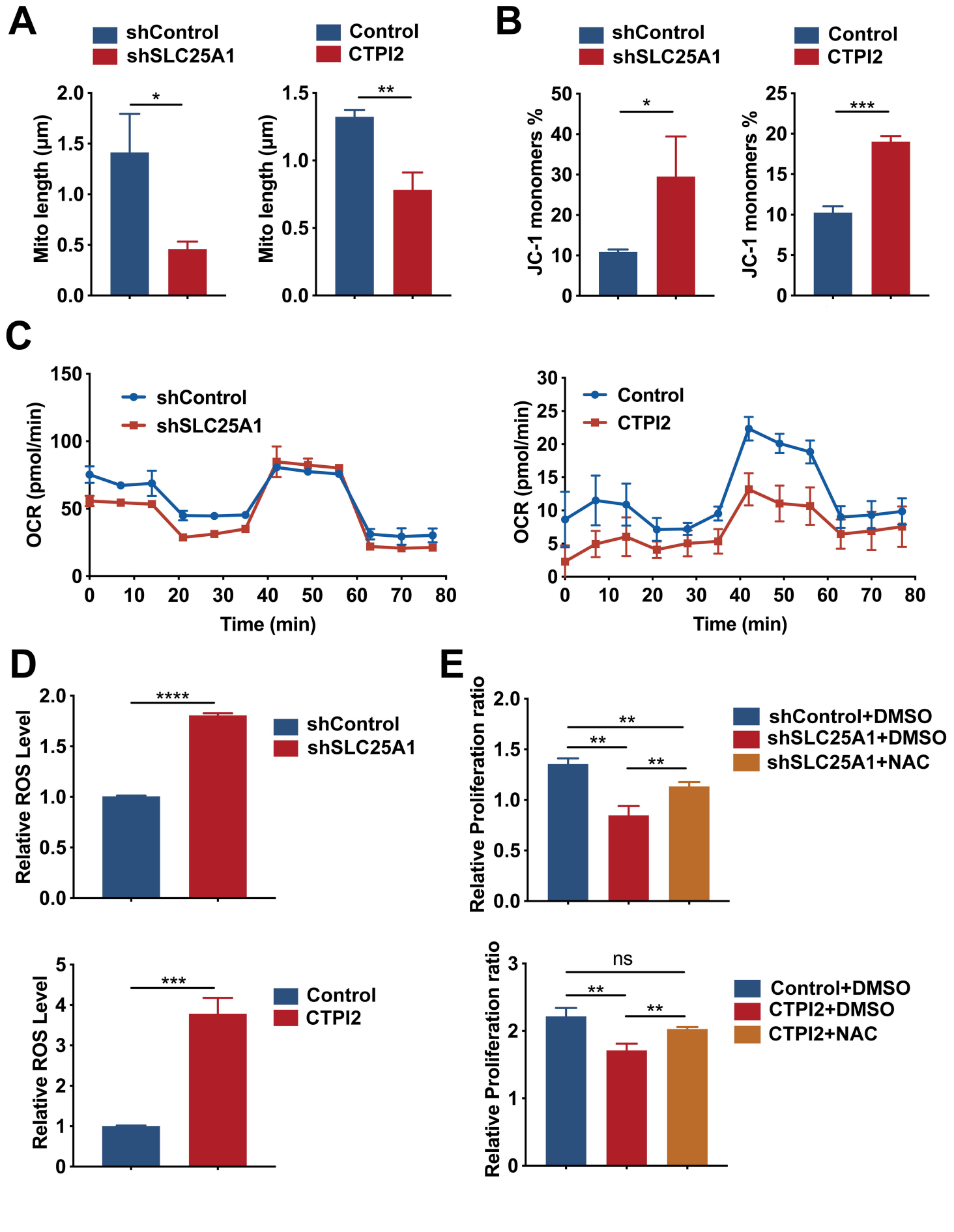
A
shControl
shSLC25A1
Mito length (μm)
2.0
1.5
1.0
0.5
0.0
*
Control
CTPI2
Mito length (μm)
1.5
1.0
0.5
0.0
**
B
shControl
shSLC25A1
JC-1 monomers %
50
40
30
20
10
0
*
Control
CTPI2
JC-1 monomers %
25
20
15
10
5
0
***
C
shControl
shSLC25A1
OCR (pmol/min)
150
100
50
0
0 10 20 30 40 50 60 70 80
Time (min)
Control
CTPI2
OCR (pmol/min)
30
25
20
15
10
5
0
0 10 20 30 40 50 60 70 80
Time (min)
D
Relative ROS Level
2.0
1.5
1.0
0.5
0.0
****
shControl
shSLC25A1
Relative ROS Level
5
4
3
2
1
0
***
Control
CTPI2
E
Relative Proliferation ratio
2.0
1.5
1.0
0.5
0.0
**
**
**
shControl+DMSO
shSLC25A1+DMSO
shSLC25A1+NAC
Relative Proliferation ratio
3
2
1
0
ns
**
**
Control+DMSO
CTPI2+DMSO
CTPI2+NAC

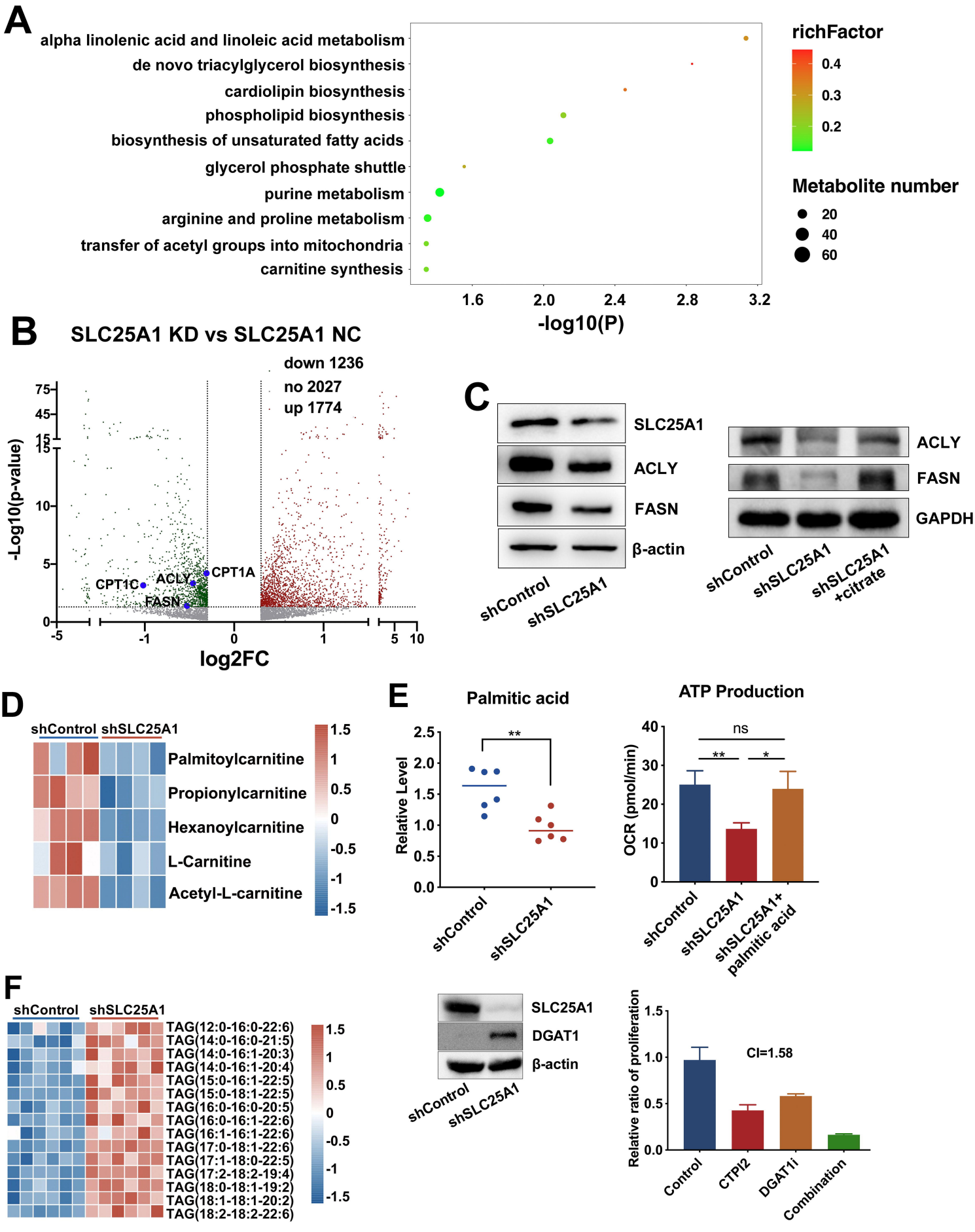
A
alpha linolenic acid and linoleic acid metabolism
de novo triacylglycerol biosynthesis
cardiolipin biosynthesis
phospholipid biosynthesis
biosynthesis of unsaturated fatty acids
glycerol phosphate shuttle
purine metabolism
arginine and proline metabolism
transfer of acetyl groups into mitochondria
carnitine synthesis
1.6
2.0
2.4
2.8
3.2
-log10(P)
richFactor
0.4
0.3
0.2
Metabolite number
20
40
60
B
SLC25A1 KD vs SLC25A1 NC
down 1236
no 2027
up 1774
-Log10(p-value)
log2FC
CPT1C
ACLY
CPT1A
FASN
C
SLC25A1
ACLY
FASN
β-actin
shControl
shSLC25A1
ACLY
FASN
GAPDH
shControl
shSLC25A1
shSLC25A1 +citrate
D
shControl
shSLC25A1
Palmitoylcarnitine
Propionylcarnitine
Hexanoylcarnitine
L-Carnitine
Acetyl-L-carnitine
E
Palmitic acid
Relative Level
shControl
shSLC25A1
ATP Production
OCR (pmol/min)
ns
shControl
shSLC25A1
shSLC25A1+ palmitic acid
F
shControl
shSLC25A1
TAG(12:0-16:0-22:6)
TAG(14:0-16:0-21:5)
TAG(14:0-16:1-20:3)
TAG(14:0-16:1-20:4)
TAG(15:0-16:1-22:5)
TAG(15:0-18:1-22:5)
TAG(16:0-16:0-20:5)
TAG(16:0-16:1-22:6)
TAG(16:1-16:1-22:6)
TAG(17:0-18:1-22:6)
TAG(17:1-18:0-22:5)
TAG(17:2-18:2-19:4)
TAG(18:0-18:1-19:2)
TAG(18:1-18:1-20:2)
TAG(18:2-18:2-22:6)
SLC25A1
DGAT1
β-actin
shControl
shSLC25A1
Relative ratio of proliferation
CI=1.58
Control
CTPI2
DGAT1i
Combination

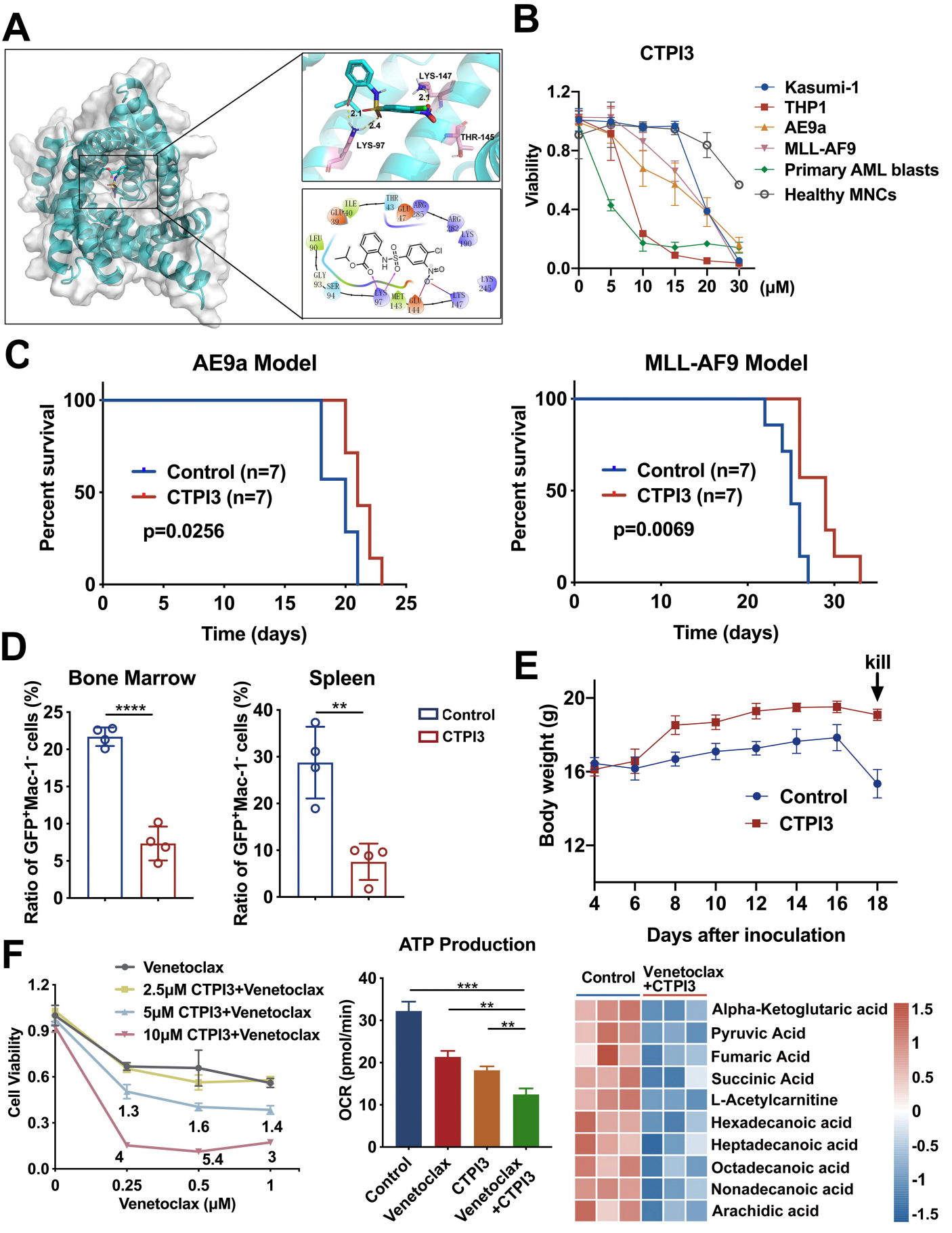
A
LYS-147
THR-145
LYS-97
B
CTPI3
Viability
(μM)
Kasumi-1
THP1
AE9a
MLL-AF9
Primary AML blasts
Healthy MNCs
C
AE9a Model
Percent survival
Control (n=7)
CTPI3 (n=7)
p=0.0256
Time (days)
MLL-AF9 Model
Control (n=7)
CTPI3 (n=7)
p=0.0069
Time (days)
D
Bone Marrow
Ratio of GFP+Mac-1- cells (%)
****
Spleen
**
Control
CTPI3
E
kill
Body weight (g)
Control
CTPI3
Days after inoculation
F
Venetoclax
2.5μM CTPI3+Venetoclax
5μM CTPI3+Venetoclax
10μM CTPI3+Venetoclax
Cell Viability
Venetoclax (μM)
ATP Production
OCR (pmol/min)
Control
Venetoclax
CTPI3
Venetoclax +CTPI3
Control
Venetoclax +CTPI3
Alpha-Ketoglutaric acid
Pyruvic Acid
Fumaric Acid
Succinic Acid
L-Acetylcarnitine
Hexadecanoic acid
Heptadecanoic acid
Octadecanoic acid
Nonadecanoic acid
Arachidic acid

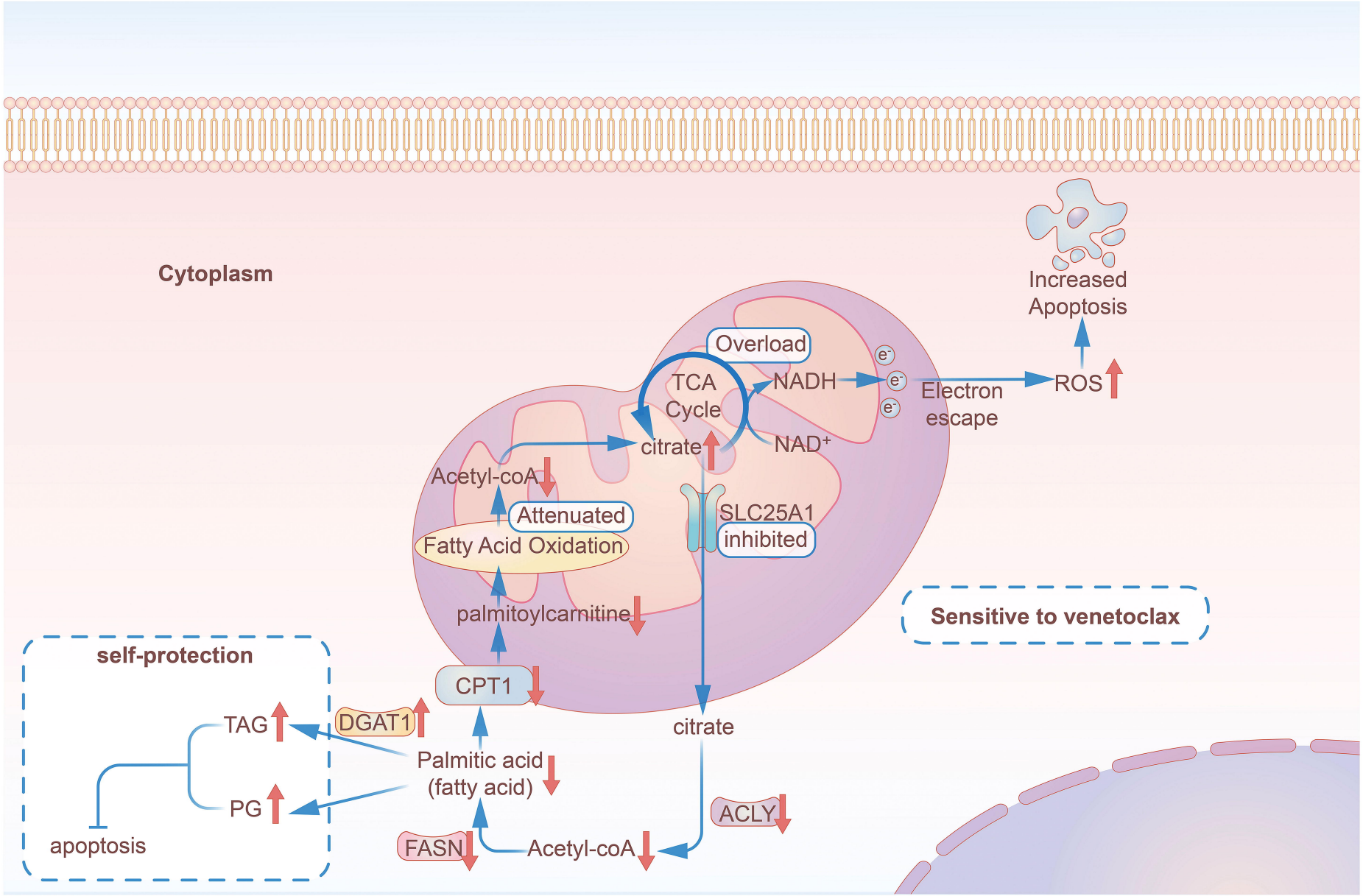
Cytoplasm
Increased Apoptosis
Overload
TCA Cycle
NADH
e-
e-
e-
Electron escape
ROS
citrate
NAD+
Acetyl-coA
Attenuated
Fatty Acid Oxidation
SLC25A1
inhibited
palmitoylcarnitine
Sensitive to venetoclax
self-protection
CPT1
TAG
DGAT1
Palmitic acid (fatty acid)
citrate
PG
apoptosis
FASN
Acetyl-coA
ACLY

Supplementary Figure Legends

Supplementary Figure 1. SLC25A1 expression profiling in AML cell lines. (A) The gene effect (chronos) of SLC25A1 knockout in various AML cell lines from DEPMAP CRISPR database. (B) The qPCR analysis of SLC25A1 expression in BM mononuclear cells from healthy donors (n=15) and AML (except M3) patients (n=69); qPCR analysis of SLC2511A1 expression in BM mononuclear cells from healthy donors (n=15) and AML patients of various subtypes, including AML1-ETO (n=11), MLL-AF9 (n=2), CBFB-MYH11 (n=3) and subtype with no fusion genes (n=39). (C) The positive ratio of SLC25A1 protein expression in BM mononuclear cells from healthy donors (n=3) and AML patients (n=3) (D) The mRNA expression of SLC25A1 in various AML cell lines from DEPMAP database. (E) The protein expression of SLC25A1 in various AML cell lines from DEPMAP database. (F) The expression levels of SLC25A1 in leukemia stem cell- negative (LSC^-) and LSC- positive (LSC^+) fractions from two independent AML datasets: GSE76009 (left) and GSE230423 (right).

Supplementary Figure 2. SLC25A1 has no effect on AML cell cycle and differentiation. (A) The RNA and protein expression of SLC25A1 was knockdown after shSLC25A1 lentiviruses transfection in Kasumi-1 and THP1 cells. (B) The colony formation assay of Kasumi-1 and THP1 cells after SLC25A1 knockdown with shControl, shSLC25A1-1 and shSLC25A1-2 lentiviruses. (C) The percentage of apoptotic leukemia cells at day 2 after SLC25A1 knockdown. (D)The cell cycle was not affected after SLC25A1 knockdown in Kasumi-1 and THP1 cells. (E) The cell

differentiation was not affected after SLC25A1 knockdown in Kasumi-1 and THP1 cells. (F) The colony formation assay of human primary AML cells (AML#5) after SLC25A1 knockdown with shControl, shSLC25A1-1 and shSLC25A1-2 lentiviruses. (G) The growth of MOLM14 and OCIAML2 cells was inhibited after SLC25A1 knockdown with shControl and shSLC25A1-2 lentiviruses.

Supplementary Figure 3. SLC25A1 KD has no effect on HL60 cells. (A) The RNA and protein expression of SLC25A1 was knockdown after shSLC25A1-1 and shSLC25A1-2 lentiviruses transfection in HL60 cells. The growth of HL60 cells was not affected after SLC25A1 knockdown. (B) The colony formation assay of HL60 cells after SLC25A1 knockdown. (C) The percentage of apoptotic leukemia cells was not affected at day 2 after SLC25A1 knockdown. (D) The cell cycle was not affected after SLC25A1 knockdown in HL60 cells. (E) The cell differentiation was not affected after SLC25A1 knockdown in HL60 cells. (F) The RNA expression of SLC25A1 was overexpression after ovSLC25A1 lentiviruses transfection in HL60. The growth of HL60 cells was promoted after SLC25A1 overexpression with ov-SLC25A1 lentiviruses. (G) The colony formation assay of HL60 cells after SLC25A1 overexpression with ovSLC25A1-1 lentiviruses. (H) The cell cycle was not affected after SLC25A1 overexpression in HL60 cells. (I) The cell differentiation was not affected after SLC25A1 overexpression in HL60 cells.

Supplementary Figure 4. SLC25A1 inhibitor (CTPI2) inhibits the growth of AML cells but has no effect on mononuclear cells from healthy bone marrow. (A) The

colony formation assay of Kasumi-1 and THP1 cells after CTPI2 application. (B) The growth of MOLM14 and OCIAML2 cells was inhibited after CTPI2 application. (C) The growth of human primary AML cells (AML#1, #2, #4, #5) was inhibited after CTPI2 application, but the growth of mononuclear cells from healthy bone marrow was not affected by CTPI2. (D) The percentage of apoptotic leukemia cells at day 1 after CTPI2 application.

Supplementary Figure 5. SLC25A1 knockdown inhibits the growth of murine AML cells in vitro and vivo. (A) The RNA and protein expression of SLC25A1 was knockdown after shSLC25A1 lentiviruses transfection in AE9a and MLL-AF9 cells. (B) The growth of AE9a and MLL-AF9 cells was inhibited after CTPI2 application. (C) The RNA and protein expression of SLC25A1 was knockdown after shSLC25A1 lentiviruses transfection in AE9a LSCs and MLL-AF9 LGMP cells. (D) The colony formation assay of AE9a LSCs and MLL-AF9 LGMPs after SLC25A1 knockdown. (E) The size changes of the spleen and liver and the weight changes of the liver in recipient mice transplanted with AE9a cells after SLC25A1 knockdown. (F) The frequencies of $GFP^{+}c\text{-}Kit^{+}$ or $GFP^{+}Mac1^{-}$ leukemia blast cells in the bone marrow, the spleen and the peripheral blood of recipient mice transplanted with shControl AE9a cells and shSLC25A1 AE9a cells. (G) The HE staining analysis of bone marrow and spleen isolated from recipient mice transplanted with shControl AE9a cells and shSLC25A1 AE9a cells.

Supplementary Figure 6. SLC25A1 KD impairs the function of mitochondria and elevates the cellular ROS level. (A) The change of mitochondrial membrane potential through fluorescence microscope after SLC25A1 knockdown or CTPI2 application in Kasumi-1 and THP1 cells. (B) The change of mitochondrial membrane potential through flow cytometry after SLC25A1 knockdown or CTPI2 application in Kasumi-1 and THP1 cells. (C) The change of mitochondrial membrane potential measured by fluorescence microscope after SLC25A1 knockdown or CTPI2 application in Kasumi-1, THP1 cells. (D) The OCRs measured by seahorse extracellular flux analyzer experiment after SLC25A1 knockdown and CTPI2 application in THP1. (E) The cellular ROS levels measured by flow cytometry after SLC25A1 knockdown and CTPI2 application in THP1. (F) The cellular ROS levels measured by fluorescence microscope after SLC25A1 knockdown or CTPI2 application in Kasumi-1, THP1 cells. (G) The growth of AML cells is rescued by ROS remover (NAC) in Kasumi-1 and THP1 transfected with shSLC25A1 and CTPI2 application.

Supplementary Figure 7. The synergistic effect of CTPI2 with venetoclax on inhibiting the growth and promoting the apoptosis in AML cells. (A) The growth of Kasumi-1 and THP1 cells with shControl or shSLC25A1 after venetoclax application. (B) The synergistic effect of CTPI2 and venetoclax on inhibiting the growth of Kasumi-1 and THP1 cells. (C) The synergistic effect of CTPI2 and venetoclax on promoting the apoptosis of Kasumi-1 and THP1 cells. (D) The synergistic effect of CTPI2 and venetoclax on elevating the ROS level of Kasumi-1 cells.

Supplementary Figure 8. SLC25A1 significantly affects fatty acid metabolism in AML cells. (A) The GO enrichment analysis of SLC25A1 related genes (R>0.5) in TCGA AML RNA sequencing database. (B) The GO enrichment analysis of SLC25A1 related genes (R>0.5) in Vizome AML RNA sequencing database. (C) The GO enrichment analysis of DEGs performed by RNA sequencing on Kasumi-1 with SLC25A1 knockdown. The GSEA performed by RNA sequencing on Kasumi-1 with SLC25A1 knockdown indicating SLC25A1 is correlated with apoptosis pathway and oxidative phosphorylation. (D) The GSEA performed by RNA sequencing on Kasumi-1 with SLC25A1 knockdown indicating SLC25A1 is correlated with fatty acid homeostasis. (E) The protein-protein interaction network of SLC25A1 by STRING online tool. (F) The protein-protein interaction network of SLC25A1 by GeneMANIA online tool. (G) The correlation curves of SLC25A1 expression and ACLY expression, or FASN expression in TCGA AML RNA sequencing database. (H) The correlation curves of SLC25A1 expression and ACLY expression, or FASN expression in Vizome AML RNA sequencing database. (I) The WB validation of SLC25A1 KD on the expression of CPT1A, CPT1C in Kasumi-1 and CPT1A, CPT1C, ACLY, FASN in THP1 cells. (J) The protein expression of CPT1A and CPT1C by three times WB after SLC25A1 knockdown in Kasumi-1 and THP1 cells. The protein expression of ACLY and FASN by three times WB after SLC25A1 knockdown in Kasumi-1 and THP1 cells. (K) The change of citrate level detected by metabolomics after SLC25A1 knockdown in Kasumi-1 cells. (L) The change of coenzyme A level detected by metabolomics after SLC25A1 knockdown in Kasumi-1

cells. (M) Palmitic acid supplementation partially rescues impaired proliferation in SLC25A1 KD cells. (N) The heat map showing the change of PG level detected by lipidomics after SLC25A1 knockdown in Kasumi-1 cells. (O) The protein expression of DGAT1 by WB after SLC25A1 knockdown in Kasumi-1 and THP1 cells. (P) The synergistic effect of CTPI2 and DGAT1i (A922500) on inhibiting the growth of THP1.

Supplementary Figure 9. Evaluation of CTPI3 efficacy and safety *in vivo.*

(A) Flow cytometry analysis of apoptosis in Kasumi-1 and THP-1 cells treated with CTPI3 for 48 hours, showing increased apoptosis cell populations compared with controls. Quantification is shown in the adjacent bar graphs. (B) *In vivo* efficacy of CTPI3 in the AE9a mouse model. Representative images of spleen size, H&E staining of spleen sections, and flow cytometry analysis of $GFP^{+}Mac1^{-}$ blasts in bone marrow (BM), spleen (SP) and peripheral blood (PB) indicate a reduction in spleen mass and infiltration of blasts upon CTPI3 treatment. (C) H&E staining of liver, kidney, and brain tissues, indicating no overt toxicity. Detection of HGB and PLT in PB and immunohistochemical staining for cleaved caspase-3 (C-caspase3) in liver, kidney, and brain tissues showing CTPI3 treatment *in vivo* with minimal systemic toxicity.

Supplementary Figure 10. Evaluation of CTPI3's combination effects with venetoclax *in vitro*. (A) Quantification of tricarboxylic acid (TCA) cycle metabolites. Relative levels of α-ketoglutarate, pyruvic acid, oxalic acid, fumaric acid, maleic acid and succinic acid were assessed to determine metabolic changes following CTPI3

treatment. (B) Expression of CPT1A and CPT1C in Kasumi-1 cells treated with CTPI3, venetoclax, or their combination, as assessed by qPCR and Western blotting. (C) Heatmap of targeted metabolomic profiling highlighting changes in fatty acid species and carnitine derivatives following single or combined treatments.

Supplementary Figure 1

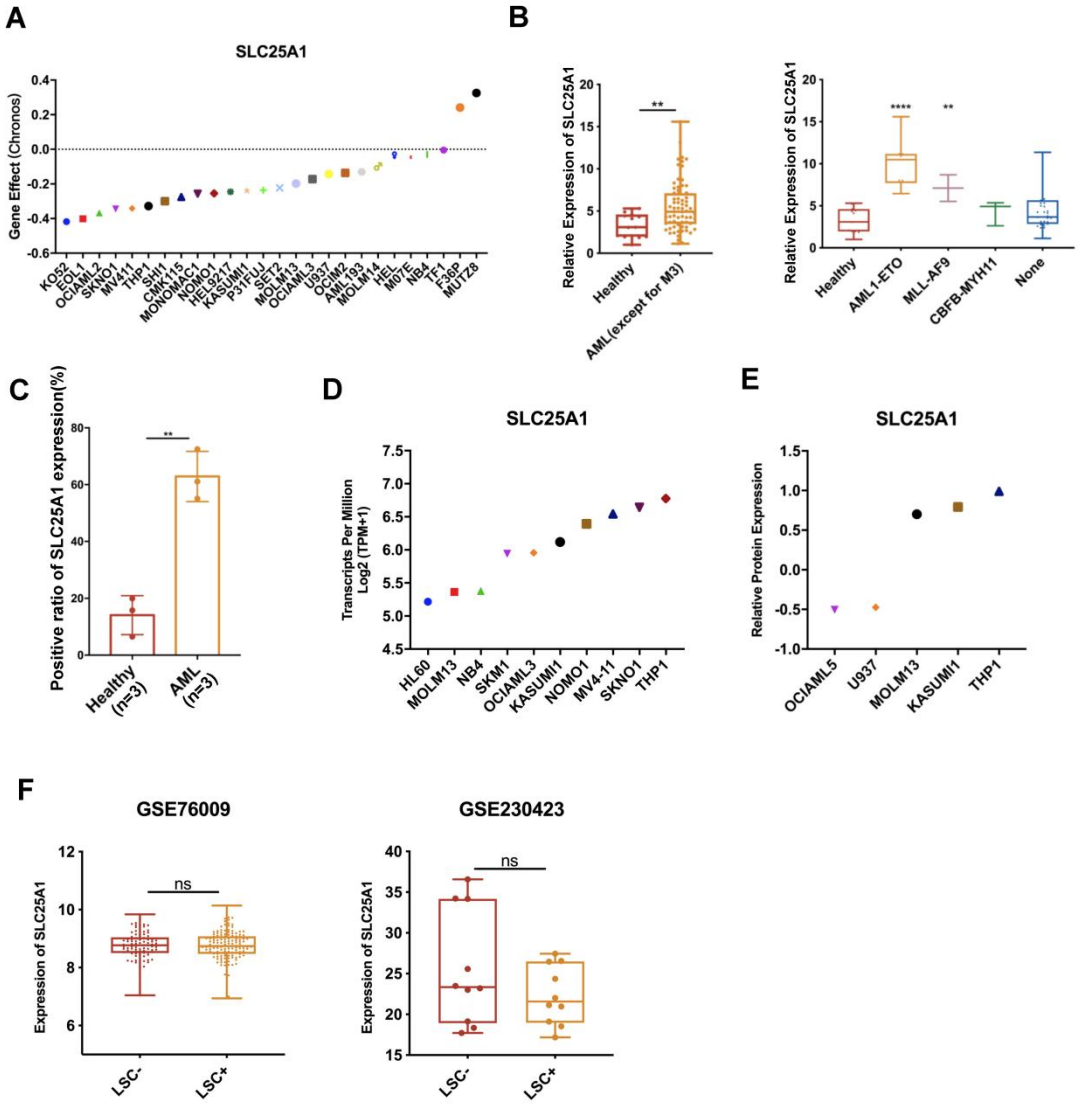

Supplementary Figure 2

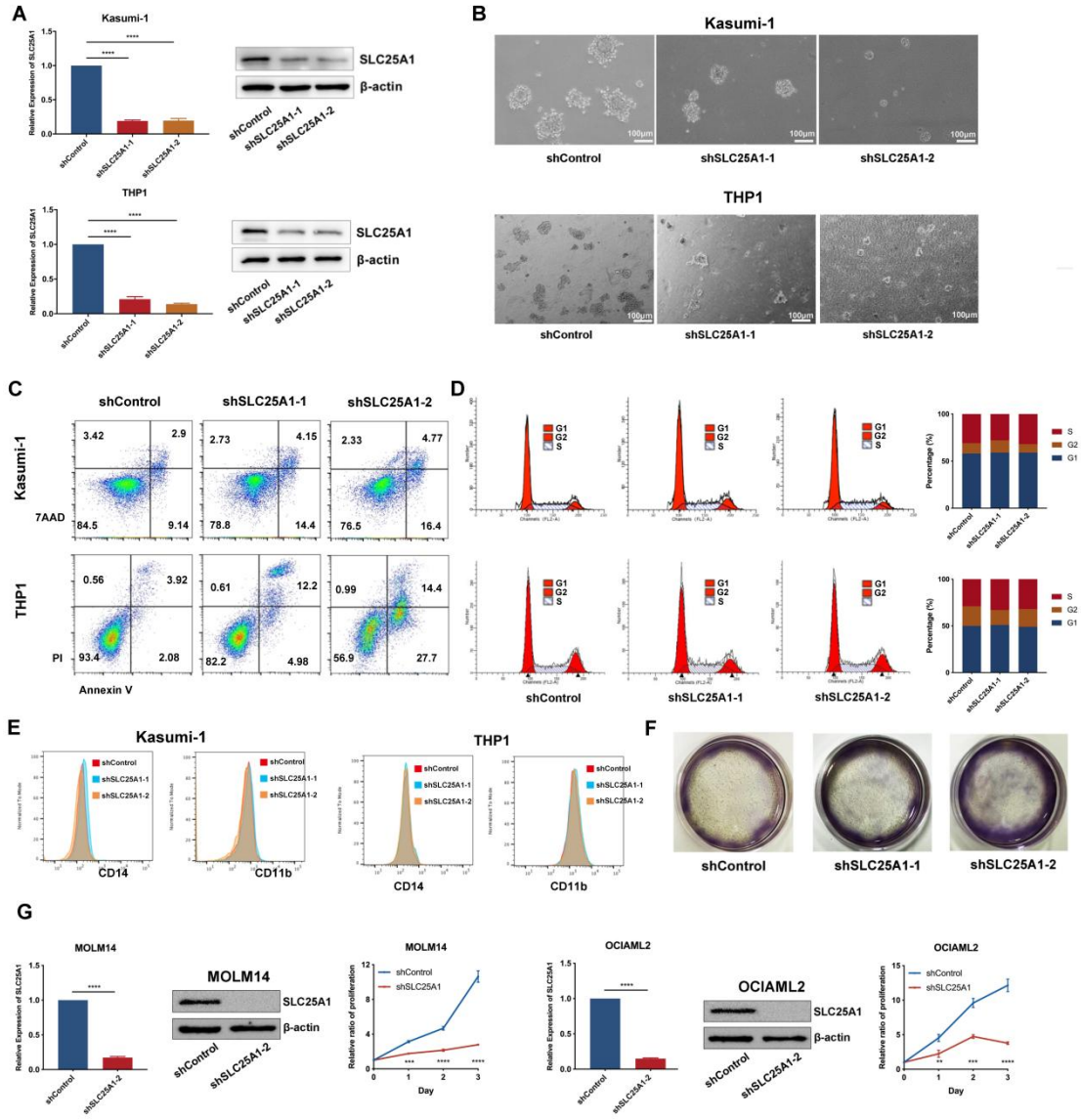

Supplementary Figure 3

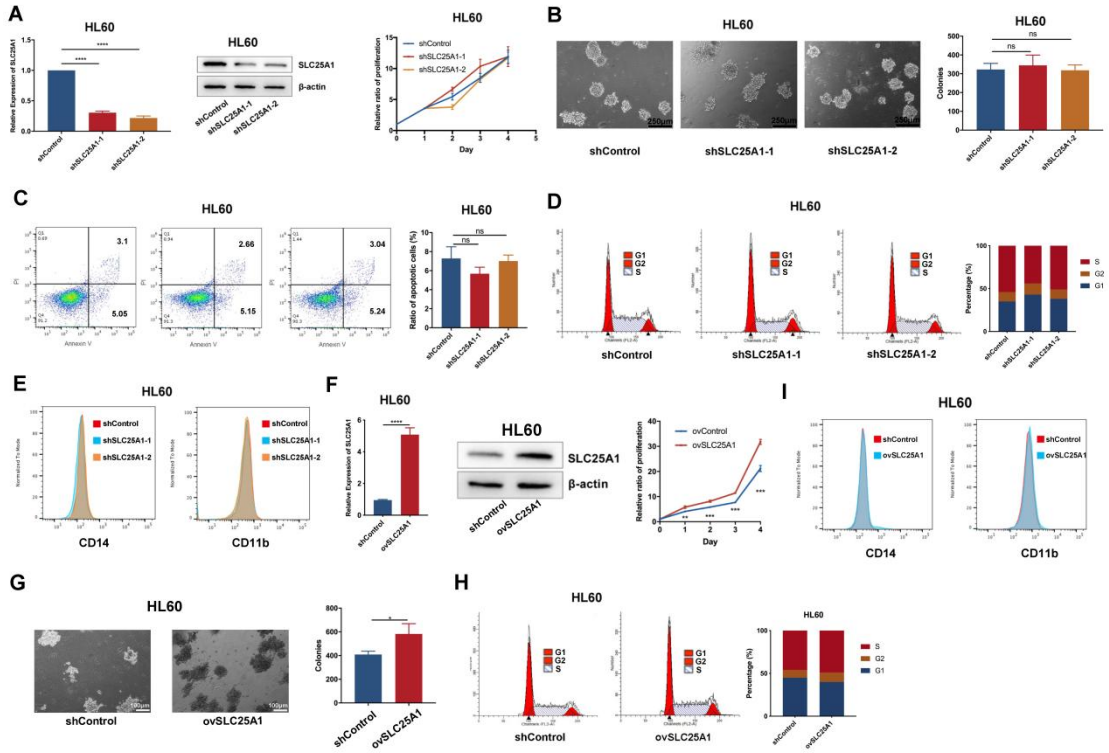

Supplementary Figure 4

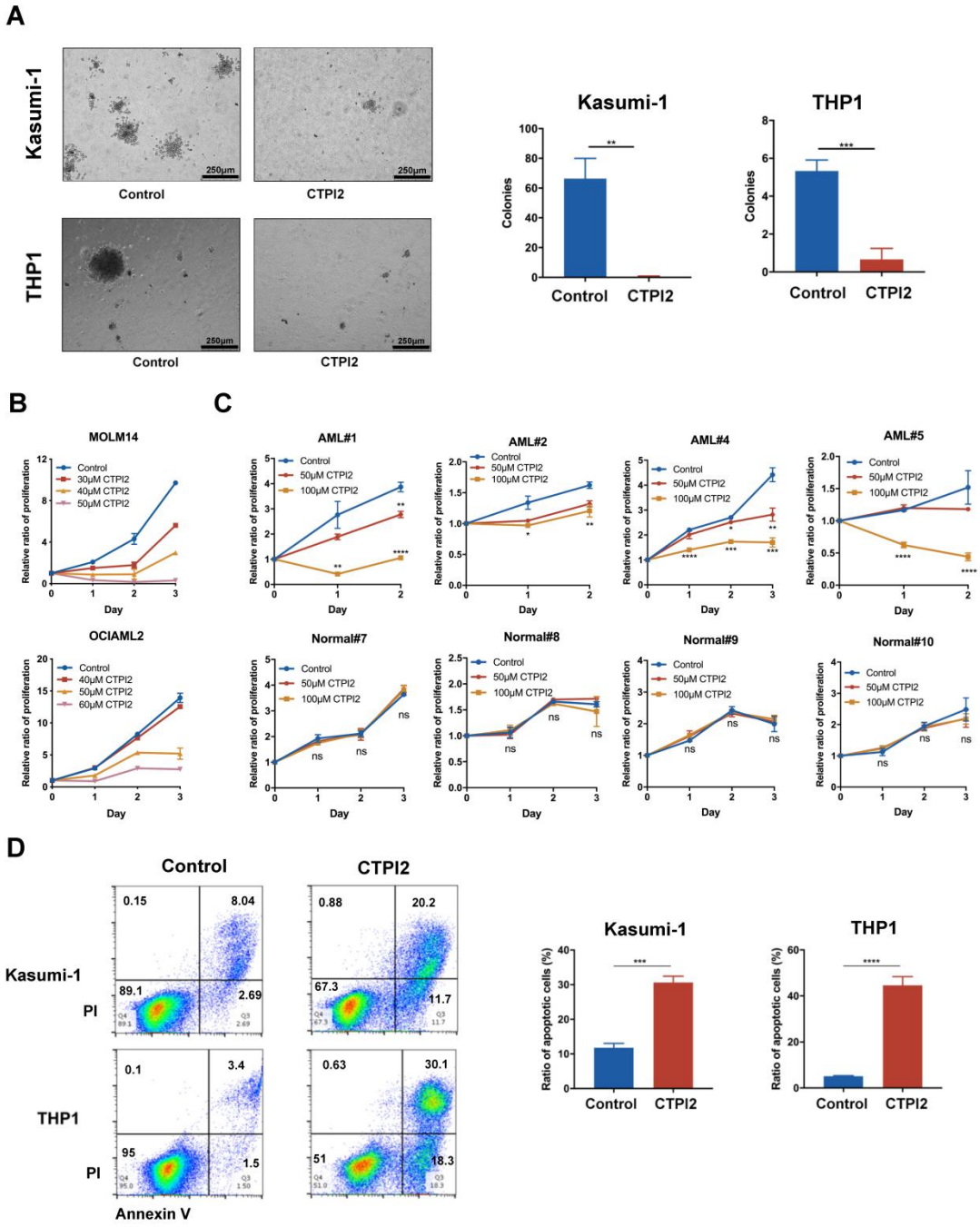

Supplementary Figure 5

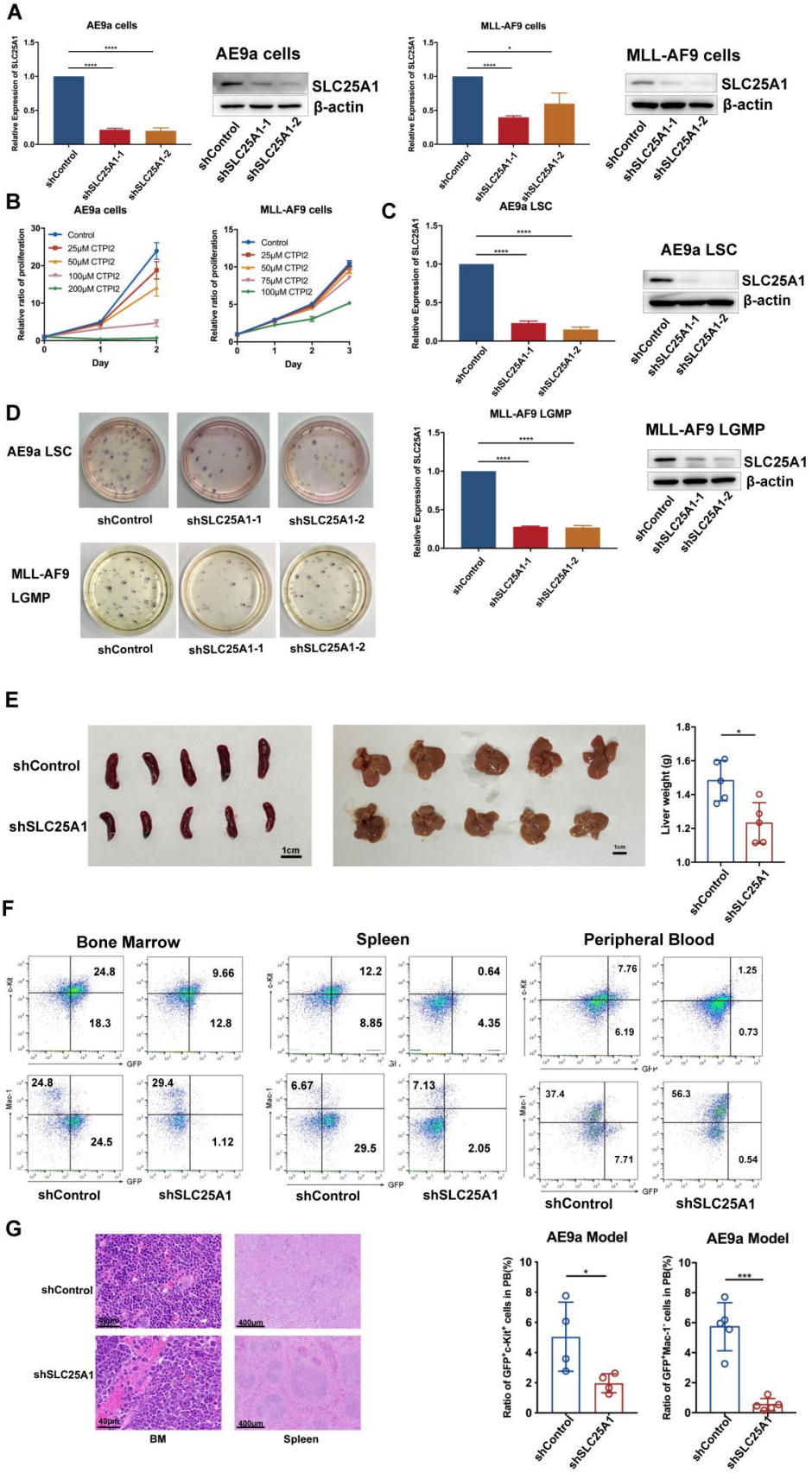

Supplementary Figure 6

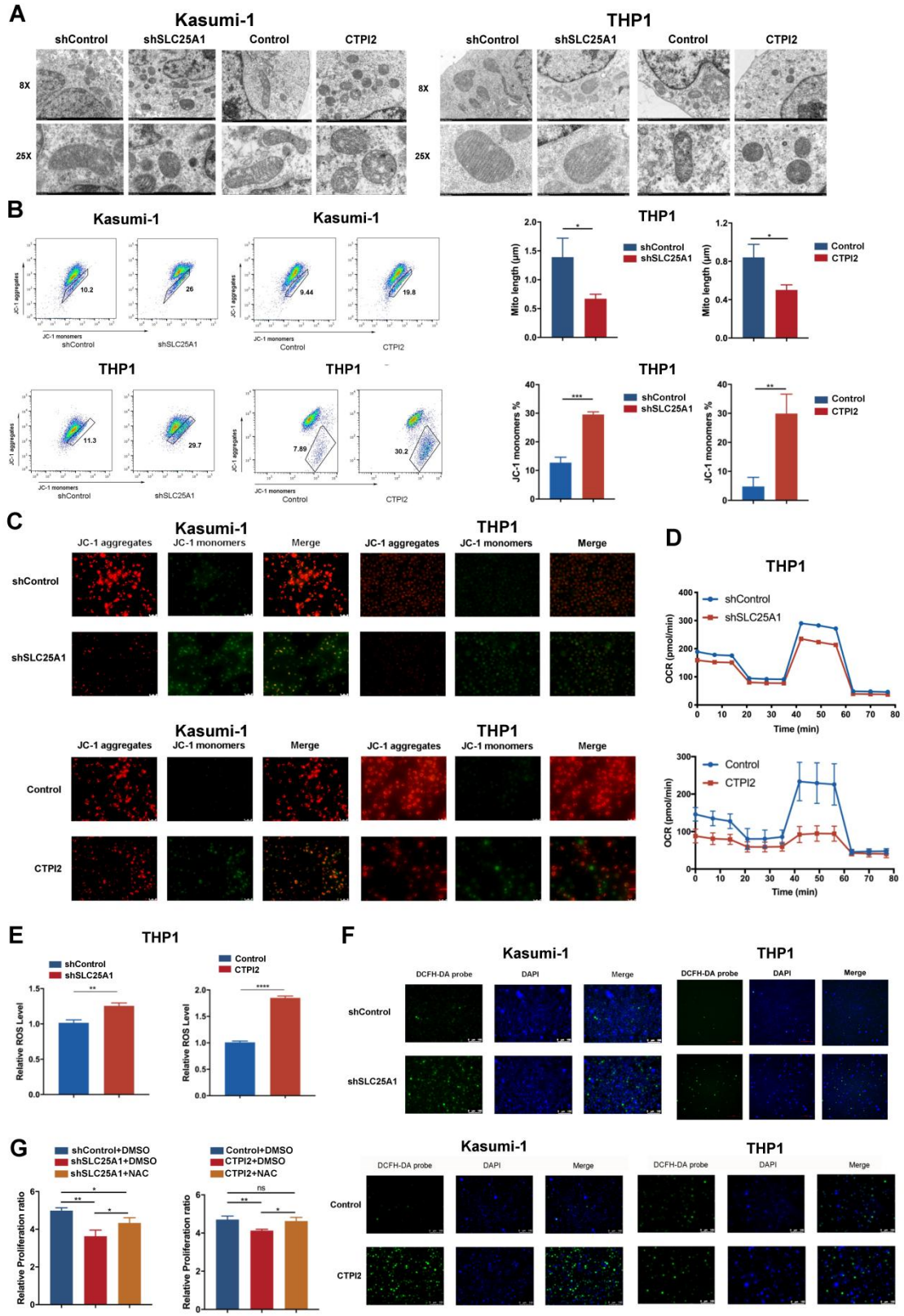

Supplementary Figure 7

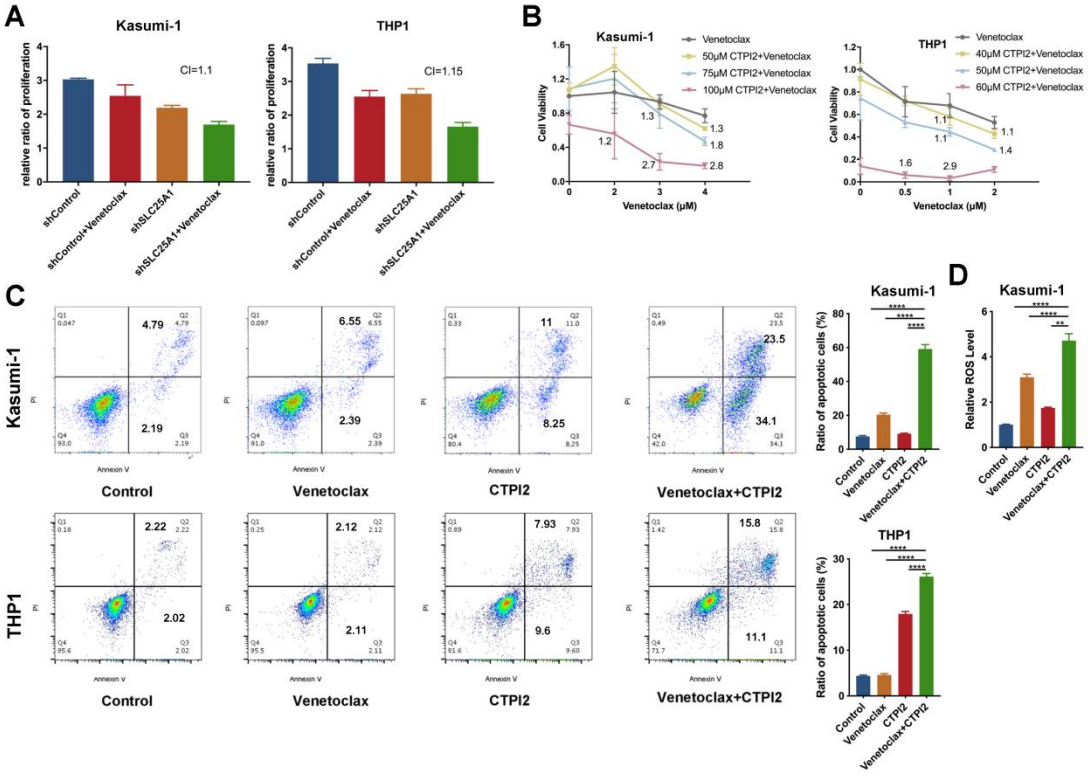

Supplementary Figure 8

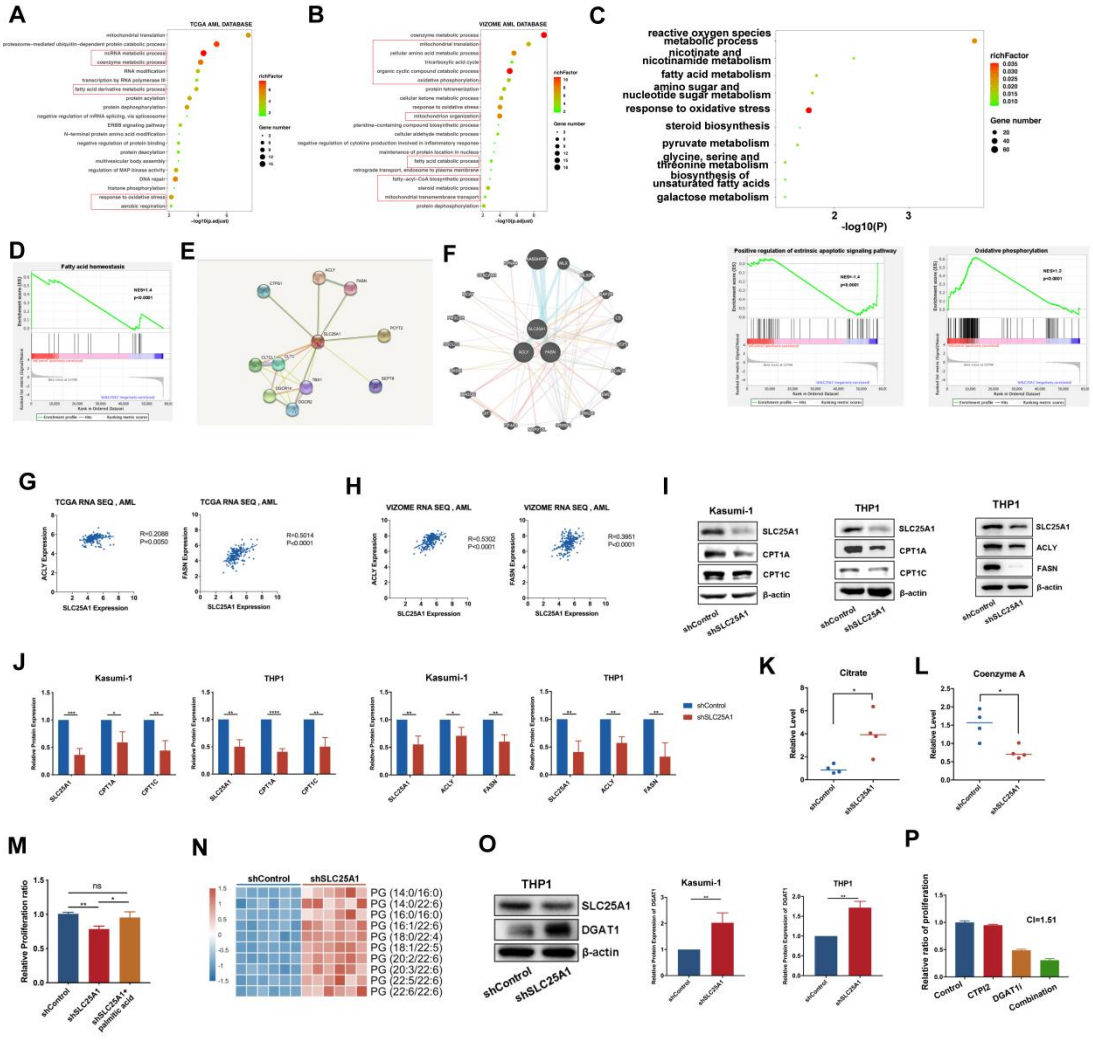

Supplementary Figure 9

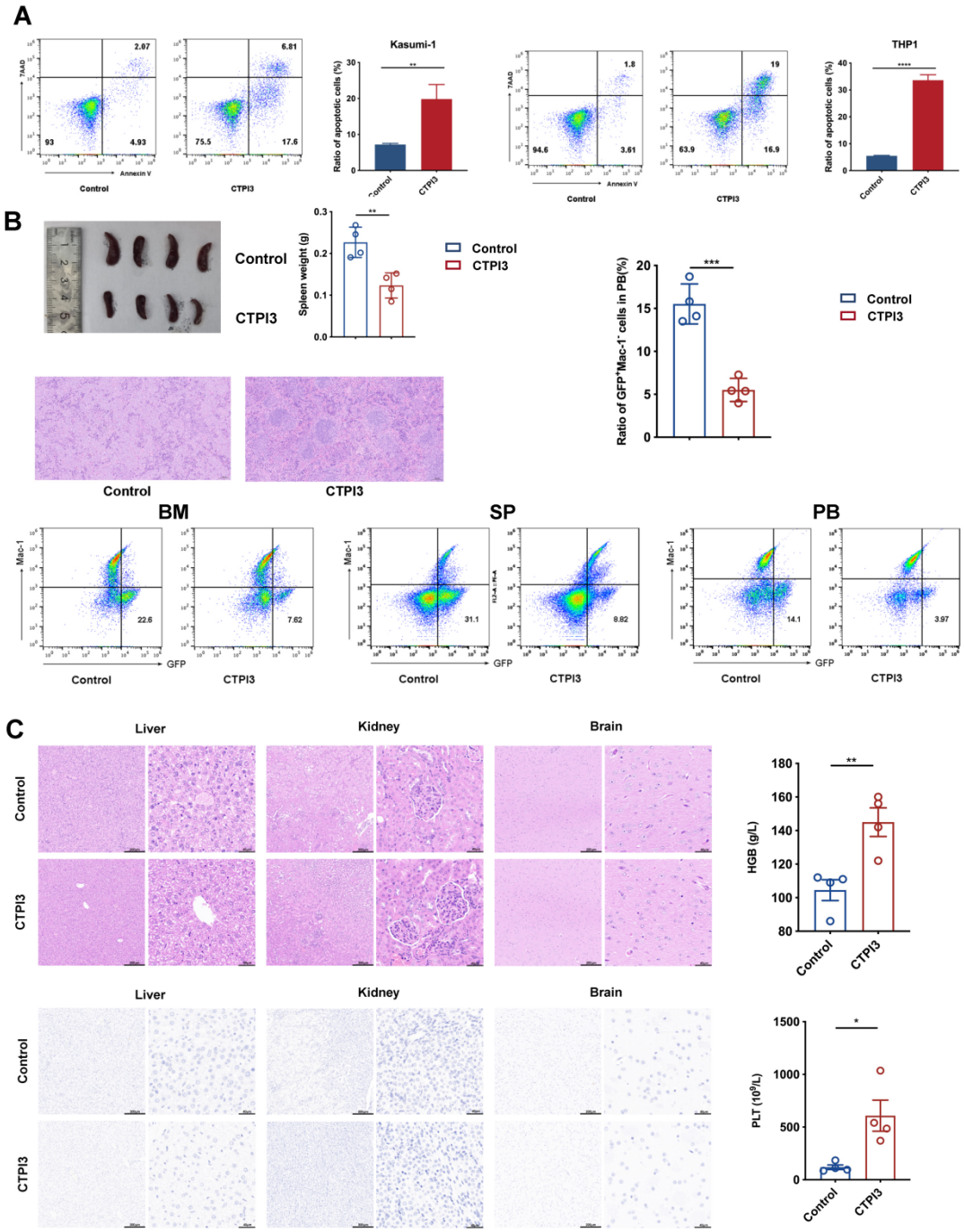

Supplementary Figure 10

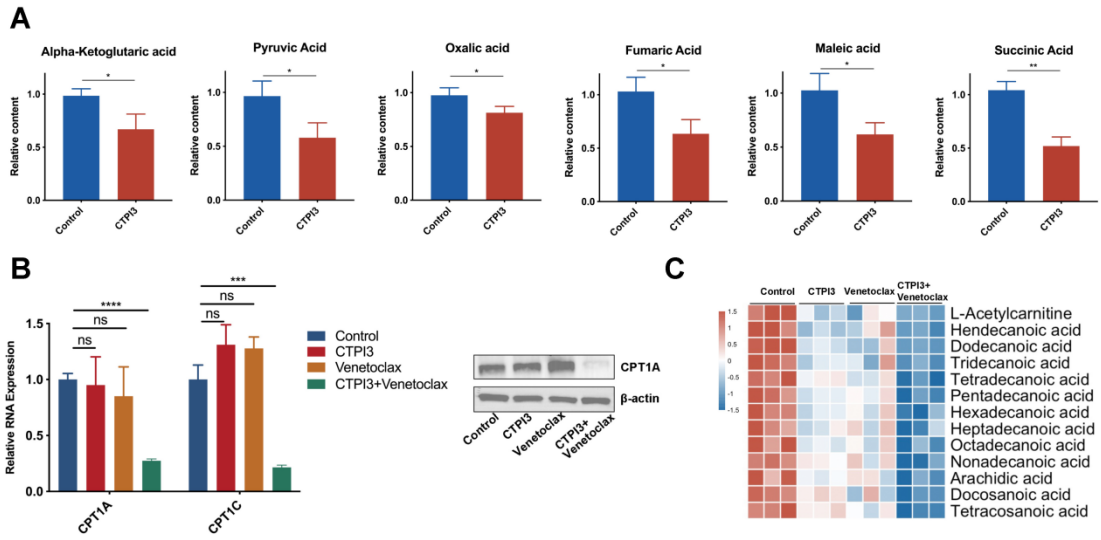

Supplemental Methods

Cell lines

The human AML cell lines Kasumi-1, THP1, HL60, MOLM14, and OCIAML2 were purchased from the Chinese Academy of Sciences cell bank (Shanghai, China). Mouse AE9a, AE9a LSC, MLL-AF9, and MLL-AF9 LGMP AML cells were obtained from Lan Wang, Shanghai Institute of Nutrition and Health. Kasumi-1, THP1, HL60, MOLM14, OCIAML2, and AE9a cells were maintained in RPMI-1640 medium containing 10% fetal bovine serum (FBS). AE9a LSC, MLL-AF9, and MLL-AF9 LGMP cells were maintained in RMPI 1640 medium containing 10% FBS, 50 ng/mL SCF, 10 ng/mL interleukin 3（IL-3) and 10 ng/mL interleukin 6 (IL-6).

Patient samples

Healthy donor samples and AML patient samples were obtained from the First Affiliated Hospital of China Medical University, with informed consent. The research was approved by the ethics committee of The First Hospital of China Medical University ([2022] Number174). Mononuclear cells (MNCs) were isolated from primary bone marrow cells using Ficoll centrifugation and maintained in RPMI-1640 medium containing 20% FBS and medium from 5637 cells.

Mice

Female C57BL/6N mice (6–8 weeks old) were purchased from Beijing Vital River Laboratory Animal Technology. All mice were bred in laminar flow cabinets under

specific pathogen-free conditions in the Laboratory Animal Center of China Medical University. Animal experiments were carried out in accordance with the China Medical University Animal Care and Use Committee guidelines.

Data Collection

Transcriptome sequencing data of 542 AML patients and 74 healthy volunteers were collected from GSE13159 (https://www.ncbi.nlm.nih.gov/geo/query/acc.cgi?acc=GSE13159). Clinical information and transcriptome sequencing data from The Cancer Genome Atlas (TCGA) in cases of AML patients were downloaded from https://xenabrowser.net. Clinical information along with transcriptome sequencing data of VIZOME were downloaded from https://www.vizome.org/ and https://www. cbiopportal.org/. AML patients' clinical information and transcriptome sequencing data of ohsu-AML were downloaded from https://www. cbiopportal.org/.

Mitochondrial membrane potential

The mitochondrial membrane potential of treated Kasumi-1 and THP1 cells was detected using a JC-1 kit with flow cytometry or fluorescence microscopy, according to the manufacturer's protocol.

Cell differentiation assay

AML cells were stained with CD11b and CD14 antibody and detected using flow cytometry.

Hematoxylin and eosin staining

Mice tissues were fixed in 4% paraformaldehyde, embedded in paraffin, and cut into 4 μM sections. The dried sections were then dewaxed and rehydrated. Hematoxylin was used to stain the nucleus, and eosin was used to stain cytoplasm. The sections were finally dehydrated and sealed.

Cell cycle assay

Cell cycle was detected using a KeyGEN Cell Cycle Analysis Kit, according to the manufacturer's protocol.

RNA extraction and reverse-transcription quantitative PCR (RT-qPCR)

Total RNA was extracted using TRIizol reagent according to manufacturer's protocol [1]. cDNA was acquired by reverse transcribing total RNA using a Prime-Script RT Master Mix Kit. RT-qPCR was performed with TB Green Premix Ex Taq II. The PCR primer sequences are list in Supplementary Table 1.

Immunohistochemistry

Bone marrow MNCs were fixed in 4% paraformaldehyde, embedded in paraffin, cut into 4 μM sections, and immunostained with streptavidin-biotin.

Western blot

Total proteins were extracted using whole-cell lysis buffer and the concentration was quantified by bicinchoninic acid assay. For each sample, 20 μg protein was loaded, electrophoresed, transferred to a polyvinylidene difluoride membrane, and blocked

with 5% skimmed milk. The membranes were then incubated with primary antibodies overnight at 4°C, followed by secondary antibodies for 1 h at 25°C. Protein expression was visualized using enhanced chemiluminescence reagents.

Cell proliferation

Cell proliferation was determined using a Cell Counting Kit-8 (CCK8), with 8×10^3 cells in each well of a 96-well plate, with 100 μL medium. CCK8 reagent (10 μL) was added directly to the plates and incubated for 2 h. The absorbance at 450 nm was then recorded. For trypan blue staining, 1×10^5 cells were plated in each well of a 6-well plate with 2 mL medium, and 10 μL of trypan blue reagent was mixed with 10 μL of medium for 3 min.

Colony-formation assay

For colony-formation assay, 5×10^3 cells were plated in 6-well plates with 1 mL Methocult GF-H4435 or Methocult GF-M3434 medium for 7–14 days.

Cell apoptosis assay

Cell apoptosis was detected using an Apoptosis Detection Kit (BD Biosciences), according to the manufacturer's protocol [1].

ROS detection assay

Cellular ROS were detected using a DCFH-DA kit with flow cytometry or fluorescence microscopy, according to the manufacturer's protocol [2].

Untargeted metabolomics

Kasumi-1 cells were infected with lentivirus expressing shRNA against SLC25A1 (scrambled shRNA as control). The metabolites were then extracted from the cells and subjected to ultra-high-performance liquid chromatography–tandem mass spectrometry (UHPLC-MS/MS) using a Vanquish UHPLC system (ThermoFisher, Germany) coupled with an Orbitrap Q ExactiveTM HF mass spectrometer (Thermo Fisher) at Novogene Co., Ltd. (Beijing, China). The raw data files generated by UHPLC-MS/MS were processed using Compound Discoverer 3.1 (CD3.1, ThermoFisher) to perform peak alignment, peak picking, and quantitation for each metabolite. These metabolites were annotated using the Kyoto Encyclopedia of Genes and Genomes (https://www.genome.jp/kegg/pathway.html), HMDB d (https://hmdb.ca/ metabolites), and LIPIDMaps databases (http://www.lipidmaps.org/).

References

1. Hu C, Chen B, Li Z, et al. Targeting UHRF1-SAP30-MXD4 axis for leukemia initiating cell eradication in myeloid leukemia. Cell research. 2022;32(12):1105-1123.

2. Shen S, Yan Z, Wu J, et al. Characterization of ROS Metabolic Equilibrium Reclassifies Pan-Cancer Samples and Guides Pathway Targeting Therapy. Frontiers in oncology. 2020;10(581197.

Supplemental Tables

Table S1 GO analysis of RNA sequence- see excel file

Table S2 GO analysis of metabolomics- see excel file

Table S3 Antibodies and Reagents

Antibody	**Brand**	**Catalog Number**
GAPDH Monoclonal antibody	PTG	60004-1
β-actin Monoclonal antibody	PTG	66009-1-Ig
HRP-conjugated Affinipure Goat Anti-Mouse IgG(H+L)	PTG	SA00001-1
HRP-conjugated Affinipure Goat Anti-Rabbit IgG(H+L)	PTG	SA00001-2
SLC25A1 Polyclonal antibody	PTG	15235-1-AP
ACLY Polyclonal antibody	PTG	15421-1-AP
FASN Polyclonal antibody	PTG	10624-2-AP
CPT1A Polyclonal antibody	PTG	15184-1-AP
CPT1C Monoclonal antibody	PTG	66072-1-Ig
DGAT1 Recombinant antibody	PTG	82945-1-RR
BD Pharmingen™ APC Mouse Anti-Human CD117 (c-Kit)	BD	567127
BD Pharmingen™ PE Mouse Anti-Human CD11b	BD	555388
Reagents	**Brand**	**Catalog Number**
Fetal Bovine Serum, qualified, heat inactivated, United States	Gibco	16140071
Penicillin-Streptomycin-Glutamine (100X)	Gibco	10378016

RPMI 1640 Medium, GlutaMAX™ Supplement	Gibco	61870036
RIPA Lysis Buffer	Beyotime Biotechnology	P0013K
Immobilon-P PVDF Membrane	Millipore	IPVH00010
Chemistar™ High-sig ECL Western Blotting Substrate	Tanon	180-5001
TRIzol™ Reagent	Invitrogen	15596026
PrimeScript™ RT Master Mix (Perfect Real Time)	TAKARA	RR036Q
TB Green® Premix Ex Taq™ II (Tli RNaseH Plus)	TAKARA	RR820Q
BD Annexin V-FITC Apoptosis Detection Kit	BD	556547
Cell Counting Kit-8	Dojindo	CK04
MethoCult H4100	STEMCELL	04100
MethoCult SF H4436	STEMCELL	04436
MethoCult GF M3434	STEMCELL	03434
Mitochondrial membrane potential detection kit (JC-1)	Beyotime Biotechnology	C2006
ROS detection kit	Beyotime Biotechnology	S0033S
Citric acid	Selleck	S5761
Palmitic acid	Selleck	S3794
Software and equipment	**Brand**	
Prism 7	GraphPad	
R version 3.4.2	R Project for Statistical Computing	

Table S4 Primer sequence

SLC25A1 RNA-F	ACGGGGTTAGGGAGATTGTG
SLC25A1 RNA-R	GCCTGCAATAGCTCCGAAGA
GAPDH RNA-F	GTCTCCTCTGACTTCAACAGCG
GAPDH RNA-R	ACCACCCTGTTGCTGTAGCCAA
mouse SLC25A1 RNA-F	GGAGAGGACTATTGTGCGGTCT
mouse SLC25A1 RNA-R	CCCGTGGAAAAATCCTCGGTAC
mouse GAPDH RNA-F	CATCACTGCCACCCAGAAGACTG
mouse GAPDH RNA-R	ATGCCAGTGAGCTTCCCGTTCAG